Testing and Experimentation of an X-Y Linear Motor

by

Irene A. Chow

Submitted to the Department of Mechanical Engineering
in partial fulfillment of the requirements for the degree of

Bachelor of Science in Mechanical Engineering

at the

MASSACHUSETTS INSTITUTE OF TECHNOLOGY

June 1992

Author .....
Department of Mechanical Engineering
May 8, 1992

Certified by .....
Kamal Youcef-Toumi
Associate Professor
Thesis Supervisor

Accepted by .....
Peter Griffith
Chairman, Departmental Committee

Testing and Experimentation of an X-Y Linear Motor

by

Irene A. Chow

Submitted to the Department of Mechanical Engineering
on May 8, 1992, in partial fulfillment of the
requirements for the degree of
Bachelor of Science in Mechanical Engineering

Abstract

A characterization study was performed on a two-dimensional linear motor. Current linear motor applications and basic linear motor concepts are presented. Two areas of motor performance were investigated. Experiments were conducted to test the effects of heat dissipation on motor temperature and platen deformation. The motor was operated for extended periods of time, and the surface temperature of the motor measured. A heat transfer model was developed to predict the temperature of the motor. Worst-case thermal deformations in the platen are also presented. The motion control capability of the motor was determined. Trapezoidal, triangular, smooth, and parabolic velocity profiles were implemented. Motor position was measured and differentiated to give experimental velocity profiles. The experimental velocity profiles were compared to theoretical profiles.

Thesis Supervisor: Kamal Youcef-Toumi
Title: Associate Professor of Mechanical Engineering

Acknowledgments

I would first like to thank Professor Kamal Youcef-Toumi for giving me the opportunity to work on this project. I have always found the research fascinating. I have enjoyed working with him, and have learned an immeasurable amount. I am grateful for the support he has given me the past nine months.

I would next like to thank Mark Brown, John Robertson, and Pedigree Petfoods. Without their support, this project would not have been possible. I am grateful to them for giving me the opportunity to work on this project.

I also appreciate the support that Paul Gjeltema has given me. He has many times taken the time to explain new concepts to me. He has helped me to resolve issues that otherwise would not concern him. His help has been invaluable, and I would not have completed this research without his support.

I would like to thank Fred Cote for helping me design fixtures and brainstorm better ways to machine parts. None of the experiments would have happened without his help.

I thank Elliot Schwartz for helping me to develop the theory behind what is happening in this motor. I appreciate the help I got from my brother, Terence Chow, in resolving the calculus necessary for describing the motions of the motor. My thanks go to John Chow and Mohsin Ansari for helping me through the differential equations I had forgotten how to solve. I appreciate the brainstorming efforts of Pablo Rodriguez in the initial stages of this research.

I appreciate the support from the guys in the Flexible Automation Laboratory at M.I.T. They provided a fun working environment. I thank Denise Robbi for her support in many areas.

Thanks go out to my great friends at Next House–Dawn Watkins, Albert Cheng, and Seth Cohen who have supported me. Thanks to Mary Hou for staying up late nights with me on Athena. I appreciate the help from Mike Rizen who has helped me be the person I am. He has always offered his support.

Last but not least, I would like to thank my parents for their unending love and

support during my past four years at M.I.T.

There is no text material missing here.
Pages have been incorrectly numbered.

Contents

1 Introduction **12**

2 Linear Motor Technology **16**

2.1 Description of Linear Motor 16

2.2 Our Linear Motor Setup 21

3 Thermal Effects **23**

3.1 Background 23

3.1.1 Heat Generation 24

3.1.2 Platen Deformation 28

3.2 Experimental Setup 31

3.2.1 Experimental Apparatus 31

3.2.2 Procedure 32

3.3 Results and Discussion 33

3.3.1 Motor Temperature 33

3.3.2 Platen Deformations 40

3.4 Conclusion 43

4 Motion Control **44**

4.1 Background 44

4.2 Experimental Setup 52

4.2.1 Experimental Apparatus 52

4.2.2 Procedure 53

4.3 Results and Discussion 54

4.3.1 Position and Velocity Profiles 54
4.3.2 Comparison of No Load Versus Loaded Velocity Profiles . . . 56
4.4 Conclusion 58

5 Conclusion **59**

A Thermocouples **61**

B Thermal Experiment Computer Programs **66**
B.1 Sample Motor Control Program 66
B.2 Data Acquisition BASIC Program 70

C Motion Control Equation Derivations **73**
C.1 Constant Acceleration Velocity Profiles 73
C.1.1 Condition for Triangular Velocity Profile 73
C.2 Linear Acceleration Velocity Profiles 74
C.2.1 General Case 74
C.2.2 Smooth Velocity Profile 75
C.2.3 Condition for Parabolic Velocity Profile 77
C.2.4 Parabolic Velocity Profile 77

D Linear Variable Differential Transformers **79**
D.1 Basic Principles of Operation 79
D.2 The DC-LVDT 80

E Motion Control Experiment Computer Programs **82**
E.1 Sample Motor Control Programs 82
E.2 Data Acquisition BASIC Program 90

F Additional Motion Control Plots **94**

List of Figures

1-1 Two-axis linear motor: forcer and platen configuration 12

2-1 Simplified Linear Motor and Platen 17
2-2 Magnetic Flux From Position One to Position Two 18
2-3 Two-Axis Forcer 19
2-4 Linear Motor Setup 21

3-1 Heat Dissipation Model 23
3-2 Elongations for Motor Travel in X and Y Directions 30
3-3 Thermal Experimental Apparatus 31
3-4 Comparison of Motor Temperatures of Various Displacements 33
3-5 Comparison of Motor Temperatures of Various Velocities, Accelerations, and Number of Active Axes 34
3-6 Comparison of Theoretical and Experimental Temperature Curves . . 37
3-7 Comparison of Theoretical and Experimental Temperature Curves . . 37
3-8 Comparison of Theoretical and Experimental Temperature Curves . . 37
3-9 Comparison of Theoretical and Experimental Temperature Curves . . 38
3-10 Comparison of Peak Temperature Change and Commanded Displacement 39
3-11 Comparison of Peak Temperature Change and Commanded Velocity . 39
3-12 Comparison of Platen Deflection and Commanded Displacement . . . 41
3-13 Comparison of Platen Deflection of Various Velocities, Accelerations, and Number of Active Axes 42

4-1 Trapezoidal Velocity Profile 45
4-2 Triangular Velocity Profile 47
4-3 Smooth Velocity Profile 48
4-4 Parabolic Velocity Profile 50
4-5 Coordinated Velocity Profile 51
4-6 Motion Control Experimental Apparatus 52
4-7 Trapezoidal Velocity Profile 55
4-8 Triangular Velocity Profile 55
4-9 Smooth Velocity Profile 56
4-10 Parabolic Velocity Profile 56
4-11 Constant Acceleration: Comparison of No Load Versus Load 57
4-12 Linear Acceleration: Comparison of No Load Versus Load 57

A-1 Seebeck Effect 61
A-2 Thermocouple Circuit 62
A-3 Thermocouple Extension Circuit 62
A-4 Thermocouple Output Versus Temperature 65

B-1 Motion Control Program: Y Direction 15 Inches, Trapezoidal Velocity Profile 67
B-2 Motion Control Program: XY Direction 8 Inches, Trapezoidal Velocity Profile 69
B-3 BASIC Temperature Data Acquisition Program 72

D-1 LVDT Operation 79
D-2 LVDT Output 80
D-3 DC-LVDT Module 81

E-1 Motion Control Program: Trapezoidal Velocity Profile 83
E-2 Motion Control Program: Triangular Velocity Profile 85
E-3 Motion Control Program: Smooth Velocity Profile 87
E-4 Motion Control Program: Parabolic Velocity Profile 89

E-5 BASIC LVDT Position Data Acquisition Program 93

F-1 Parabolic Velocity Profile: Position and Velocity Plots 94

F-2 Parabolic Velocity Profile: Position and Velocity Plots 95

F-3 Trapezoidal Velocity Profile: Position Plots for Loaded and Unloaded 95

F-4 Triangular Velocity Profile: Position Plots for Loaded and Unloaded . 95

F-5 Smooth Velocity Profile: Position Plots for Loaded and Unloaded . . 96

F-6 Smooth Velocity Profile: Position Plots for Loaded and Unloaded . . 96

List of Tables

3.1 Thermal Test Settings and Peak Temperatures 33

3.2 Theoretical Peak Temperatures 36

3.3 Platen Deflection 40

4.1 Trapezoidal Profile Characteristics 46

4.2 Triangular Profile Characteristics 48

4.3 Smooth Profile Characteristics 49

4.4 Parabolic Profile Characteristics 50

4.5 Motion Control Experiments 54

A.1 Common Thermocouple Characteristics 64

Chapter 1

Introduction

The Sawyer linear motor, invented in 1969, consists of a "forcer" mechanism which moves about a platen [16]. The platen can either be one-axis or two-axis. Figure 1-1 illustrates a simplified two-axis linear motor [13]. It operates as a permanent magnet rotary stepper motor which has been rolled out flat. The forcer is the analog of the rotor, and the platen is the analog of the stator. The platen is as long as the desired length of motion. As in a rotary dc motor, motion in a linear motor is generated

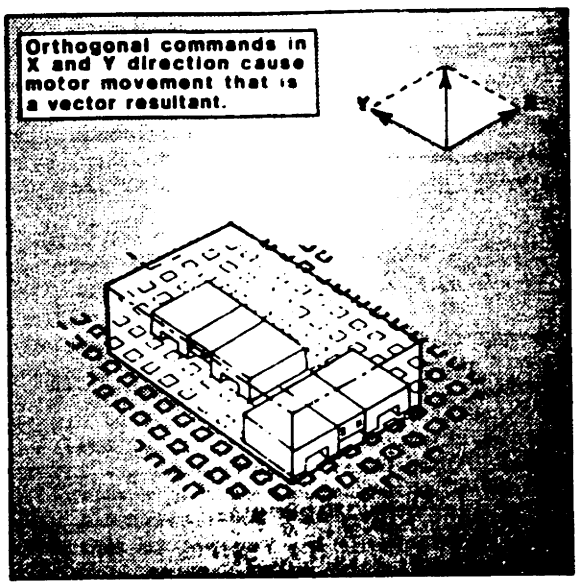

Figure 1-1: Two-axis linear motor: forcer and platen configuration

by changing the currents in electromagnetic windings. An air or contact bearing separates the forcer from the platen. For each axis, the forcer mechanism consists

of two electromagnets with toothed pole faces bridged by a permanent magnet. The platen is etched with teeth matching the pitch of the electromagnets. To create a two axis motor, forcer mechanisms are placed orthogonal to one another. The platen is etched in a waffle pattern such as the one shown in Figure 1-1. Tooth pitches are typically 0.020" (0.0508 cm) or 0.040" (0.1016 cm).

Linear motors are direct positioning motors: there is no mechanical interface (lead screws, belts, etc.) between the platen and the forcer. Therefore they are capable of high speeds and accelerations (currently over $1\frac{m}{s}$ and over $1g$). These characteristics give the motor almost frictionless motion and reliable open-loop performance. The motor can be stepped at one-quarter of the pitch. Microstepping gives even greater resolution. Current applications include precise part manipulation. Xynetics, Inc. developed the "Automated Drafting System" [16]. This system consists of a two-axis linear motor running on a platen above the motor. The motor moves a drafting head fixed to the forcer. Another Xynetics application is a laser fabric cutting system. Instead of using a two-axis linear motor, it uses three one-axis linear motors [16]. The laser head is fixed to one forcer. The ends of the corresponding platen of this axis are each fixed to another forcer, whose travel are perpendicular to the first. The third application is in the area of micro-electronics assembly. Two-axis motors are implemented in pick and place systems. In this case, one advantage of linear motors is that a single platen can have multiple forcers operating on it. The programmed motions must insure collision avoidance and prevention of power supply cord entanglements. The resolution and open-loop accuracy capable of the linear motor makes it ideally suited for these applications.

The linear motor system being studied applies its capabilities to high-speed packaging. Although linear motor systems have been implemented in high-speed micro-electronics assembly, the loads are small. With load as light as chips and microprocessors, the linear motor has no problem reaching accelerations of $1g$ and velocities of $1\frac{m}{s}$. The capability of the linear motor to reach these values changes as the load on the motor increases. The other requirement the system being studied has is a high throughput rate. It requires developing a motor that will maintain high velocities

and accelerations with the increased load. To make these improvements, the current capabilities of the motor must be first be understood.

The purpose of this study was to characterize the linear motor in two main areas. The first area is the thermal characteristics of the motor. The motor generates heat as it moves. The motor requires power to maintain position even if it is not moving. Current flows through the resistance of the electromagnetic coils generating heat. The implications of the heat generated include reduced motor performance and deformations to the platen. The motor has a rated peak temperature at which it should operate. One outcome of this study was the identification of the peak temperature in the forcer when operating following different geometrical paths along the platen. Since the forcer is traveling along the platen, heat is transfered from the forcer to the platen. This study revealed the effects to the platen of extended use of the motor. The platen acts as a heat sink; the heat transfered results in deformations of the platen. These deformations affect the positioning accuracy of the motor. The eventual application of these studies is to assess the need for a system to reduce the thermal effects. If air bearings are used, cooling is provide; but perhaps not enough.

The second area of study was the motor motion control. Currently linear motors are operated open-loop. The purpose of this part of the characterization study was to determine the accuracy of the open-loop system. The motor is commanded to move to a specified position using a particular velocity profile to get there. This study revealed the accuracy to which the motor could execute the command. By measuring the position of the motor following a command, the position accuracy and the velocity profile could both be determined. The results of this study can be used to assess the possibility of position or velocity feedback for closed-loop control of the linear motor.

Although the two areas of study seem disparate, they both contribute to a better understanding of the motor. These results may be used to develop the motor to allow it to reach higher speeds and accelerations with greater accuracy; perhaps through feedback control. Chapter 2 discusses linear motor technology and the application of the linear motor used in the studies. Chapter 3 discusses the theory and results of the thermal characterization of the motor. It describes the causes of the heating of

the motor as well as the implications of the heating. Chapter 4 discusses the motion control aspects of the motor. It describes the various velocity profiles possible and the positional accuracy of the motor. Chapter 5 offers conclusions and implications of the studies conducted.

Chapter 2

Linear Motor Technology

2.1 Description of Linear Motor

The linear motor used in the experiments consisted a Northern Magnetics, Inc. two-phase, two-axis forcer suspended from a 52" (1.3208 m) x 37" (0.9398 m) platen. The bearing between the platen and the forcer is an air cushion from shop air at $80psi$ (3830 $\frac{N}{m^2}$). However, the description of the motor will focus on a one axis forcer. The two-axis forcer is a combination of orthogonal one-axis forcers. Figure 2-1 shows a simplified version of the motor and the platen.

The forcer consists of two electromagnets bridged by a permanent magnet. The detail of the toothed faces of the electromagnets is not shown in Figure 2-1. The pitch of the electromagnet pole faces equals that of the platen (typically 0.020" (0.0508 cm) or 0.040" (0.1016 cm). However, the pole faces are distanced 1.5 times the platen tooth spacing. The distance between the two electromagnets is 1.25 times the platen tooth spacing. This configuration allows for only one of the pole faces to be completely aligned with a platen tooth at a given time.

Motion is generated by commutating the magnetic flux through particular legs of the electromagnets. Figure 2-2 shows the flux lines from one configuration to the next.

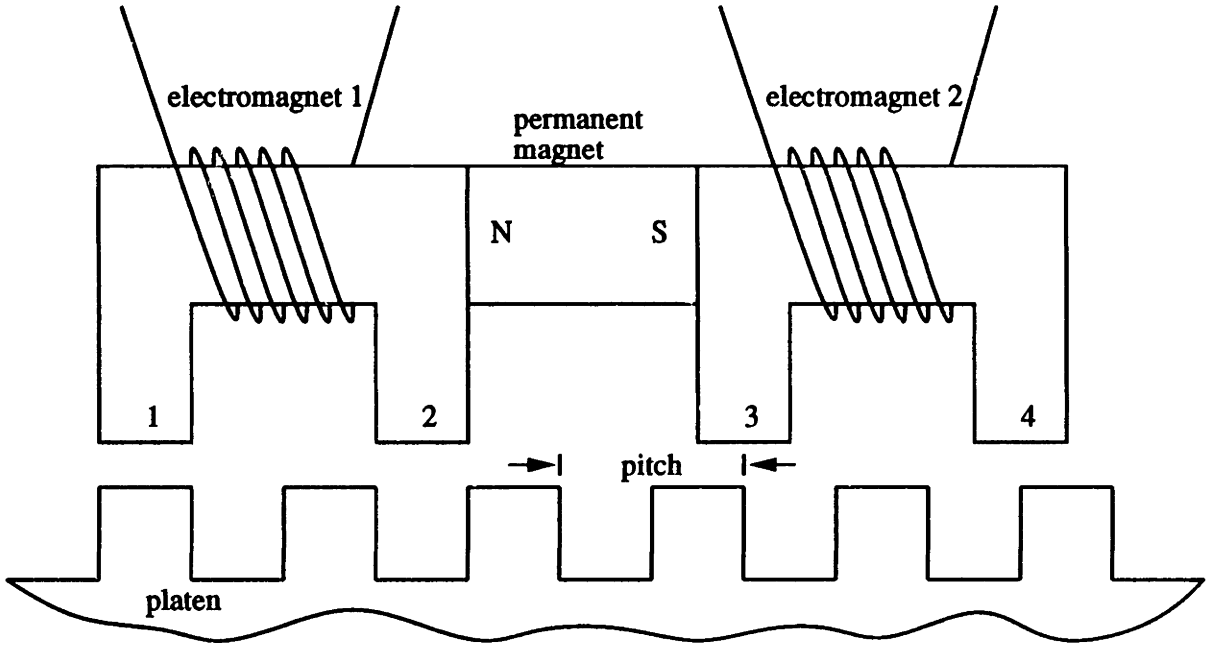

Figure 2-1: Simplified Linear Motor and Platen

Figure 2-2 A shows the magnetic flux with no coil current. The flux lines of the permanent magnet flow through one electromagnet, cross the air gap, travel through the platen, and back through the other electromagnet. The flux is divided between the legs of the electromagnet. This figure also represents the flux when the current input is constant. Figure 2-2 B shows the full coil current excitation that commutes the flux entirely through electromagnet leg 1. The positive current in coil 1 generates magnetic flux in one direction. It increases the flux through leg 1 and cancels the flux in leg 2. The commutation of the coil flux through a particular leg causes a tangential force which drives the forcer to align that leg with a platen tooth because the magnetic flux seeks to minimize its path reluctance. Therefore electromagnet leg 1 lines up with a platen tooth.

Figures 2-2 C and D show the flux paths necessary to initiate forcer motion to the right. In Figure 2-2 C, the current is positive in coil 2. The flux is canceled in leg 3 and commutated entirely through leg 4, aligning leg 4 with the next platen tooth. In Figure 2-2 D, the current through coil 1 is negative. The current is commutated entirely through leg 2. The next step would be to commutate the current through leg

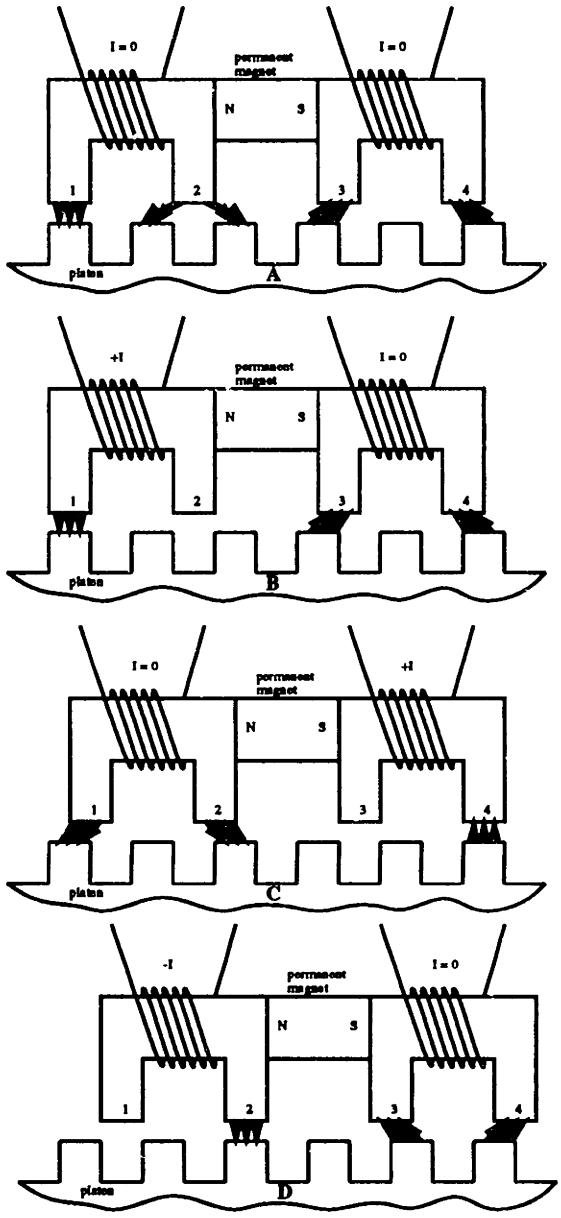

Figure 2-2: Magnetic Flux From Position One to Position Two

3 by exciting coil 2 with negative current. Finally, commutating the current through leg 1 would lead the forcer to a position exactly one platen tooth to the right of where it started in Figure 2-2 B. By repeatedly changing the electromagnetic winding currents in this sequence, the forcer moves along the platen continuously. The driving currents are actually two sinusoids 90 degrees out of phase. Each sinusoid drives the current in each of the two electromagnets. A motor with this input is a two-phase motor. Since it takes 4 "steps" for the forcer to move one tooth pitch, one *cardinal* step is one-quarter of the platen tooth pitch. Greater resolution can be achieved by

microstepping the motor.

The magnetic field created also results in normal forces of attraction between the forcer and the platen. The air bearing offsets the attractive force to allow for nearly frictionless motion. The air gap between the forcer and the platen is approximately 0.0008" (0.002032 *cm*).

To create a two-axis linear motor, two single-axis motors can be placed orthogonal to one another such as shown in Figure 1-1. However, the motor shown in Figure 1-1 would have serious dynamic problems. Since both axes must have a degree of intimacy with the platen, they must be placed next to each other. The force vector of only one of the axis would be able to pass through the center of mass of the motor. When the other axis commands a displacement, it would also command a rotation about the center of mass. Since the operation of the motor is critically dependent on its alignment with the platen teeth, this motor would not work. The solution to this problem is shown in Figure 2-3.

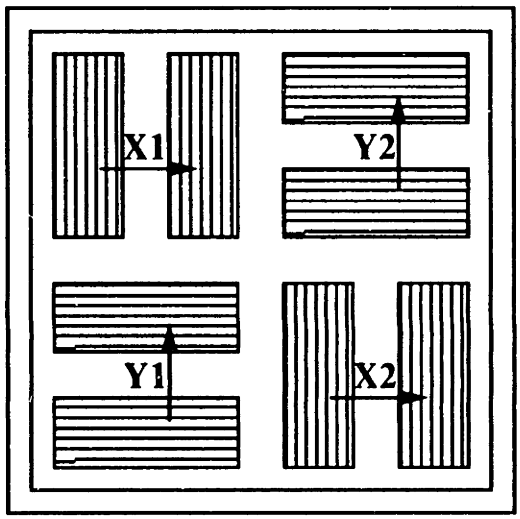

Figure 2-3: Two-Axis Forcer

The motor actually uses two sets of forcers for each axis. By configuring them in such a way, if both forcers are commutated in parallel, there is no moment about the center of mass of the motor (assumed to be at the center of the motor). The problem of rotation is eliminated. Figure 2-3 is a representation of the actual motor used in

the experiments. The two-axis platen looks like a waffle iron with alternating peaks and valleys spaced at the tooth pitch. The platen is made of steel, with the valleys of the teeth chemically etched. The valleys are filled with a magnetically and electrically nonconductive polymeric material. The surface is surface ground to achieve a smooth level surface.

2.2 Our Linear Motor Setup

The experimental setup is shown in figure 2-4 [17].

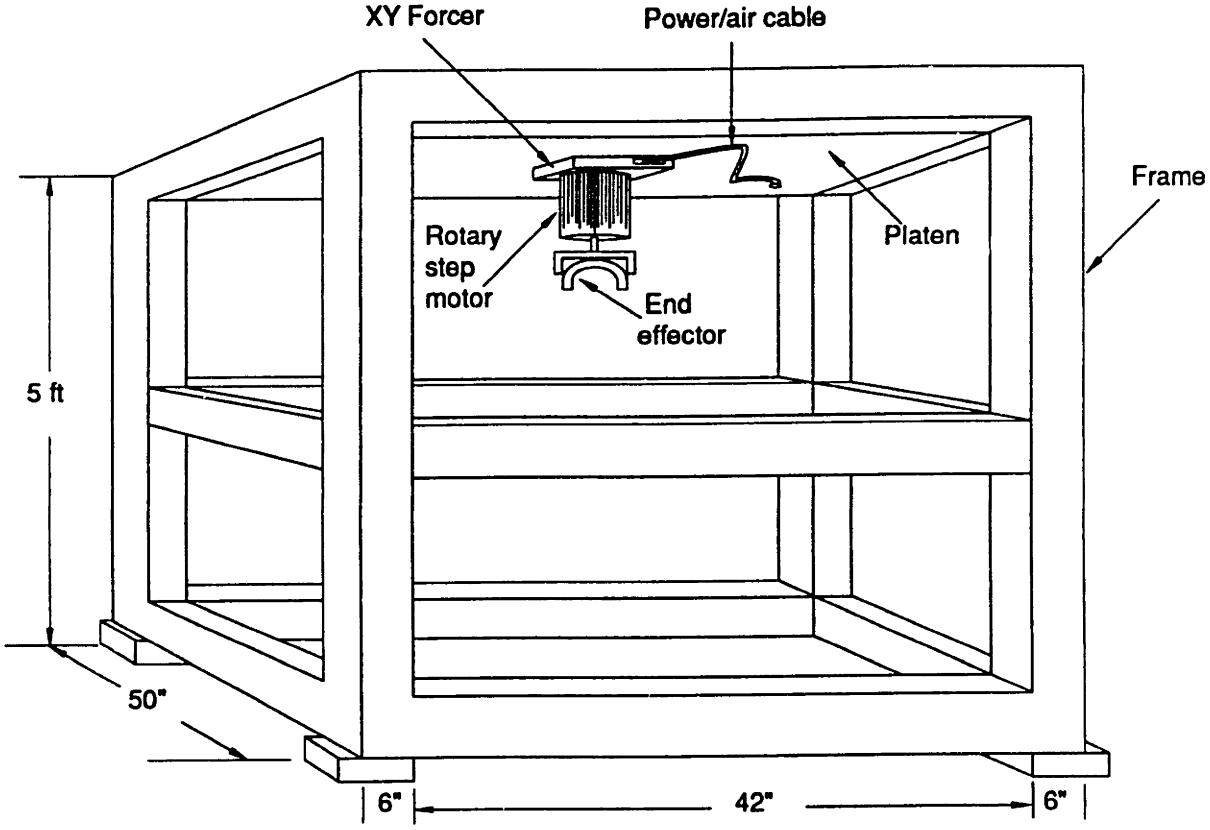

Figure 2-4: Linear Motor Setup

The main components of the setup used consisted of a two-dimensional forcer suspended from a platen. The forcer used was a two-phase, two-axis Northern Magnetics Model 4SY2504-2-0. The platen was supported by a steel frame. Four micro-switches bolted to two opposing corners of the motor served as limit switches. A rotary stepper motor secured to the bottom of the forcer added a third rotational degree of freedom. An end-effector fastened below the rotary motor moved a payload in the X-Y plane. Two modular end-effectors could be interchanged: an electromagnet and a push mechanism. The end-effectors manipulated the payloads to be packaged.

An umbilical to the forcer supplied shop air for the bearing, connections to limit switches, and power and logic to the rotary stepper motor, the electromagnetic end-effector, and the forcer itself. The motor driver was a Motion Science Two-axis Micro Step Motor Drive. The driver had a capability of microstepping up to 125

microsteps per full step (with one full step corresponding to a cardinal step of one-quarter platen tooth pitch). A PC compatible computer housed the controller card, a Motion Science MoPro IIPC. All control programs were written in a high-level motion control language included in the software provided with the MoPro IIPC card.

Chapter 3

Thermal Effects

3.1 Background

Applications of the linear motor will require the motor to run continuously. The current applied to the motor's resistive coils generates heat. The presence of continuous heat dissipation from the coils causes deformations to the platen. These deformations reduce the accuracy of the motor. The purpose of the temperature experiments was to verify a model for predicting the heat dissipated and to assess the effects to the platen.

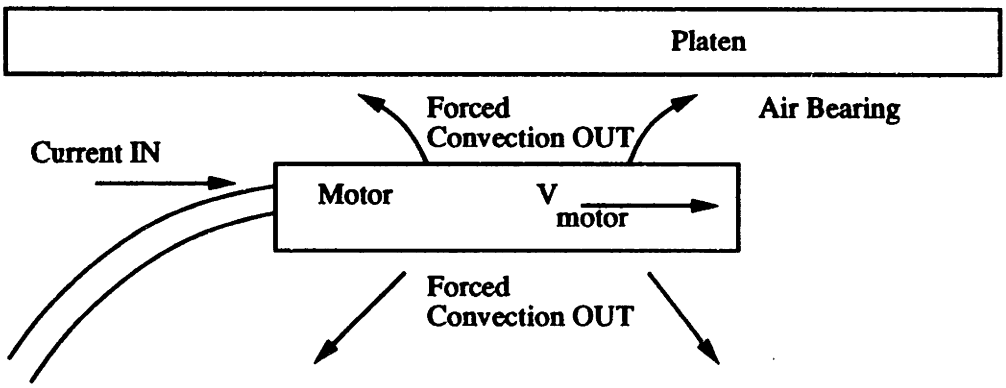

Figure 3-1: Heat Dissipation Model

3.1.1 Heat Generation

In order to develop a model for the heat dissipation of the motor, several assumptions were made. Figure 3-1 shows a schematic of the model used for predicting the motor temperature. The motor was assumed to be a solid block of aluminum with uniform temperature. The motor had an even heat distribution following the equation:

$$\frac{\partial T_m}{\partial x} = \frac{\partial T_m}{\partial y} = \frac{\partial T_m}{\partial z} = 0 \tag{3.1}$$

where T_m is the temperature of the motor, and x, y, and z are coordinates in three dimensions. The energy storage capacity $\dot{E}_m$ of the motor is given by:

$$\dot{E}_m = \rho c_p \frac{\partial T_m}{\partial t} dx dy dz, \tag{3.2}$$

where ρ is the density of aluminum, c_p is specific heat at constant temperature of aluminum, and t is time. Since the motor has a uniform temperature distribution, equation 3.2 becomes:

$$\dot{E}_m = \rho c_p \frac{\partial T_m}{\partial t} dV \tag{3.3}$$

$$= m c_p \frac{dT_m}{dt}, \tag{3.4}$$

where m is the mass of the motor. Since no temperature gradient across the motor is assumed, there is no heat transfer by conduction.

The current to the motor provided the only heat source into the system. The current through resistance of the coils generated heat according to:

$$q_1 = P_R = IV = \sum I^2 R = I_{x1}^2 R_{x1} + I_{x2}^2 R_{x2} + I_{y1}^2 R_{y1} + I_{y2}^2 R_{y2}, \tag{3.5}$$

where q_1 is the heat transfer rate in Watts, P_R is the power through the coils, I_{x1}, I_{x2}, I_{y1}, and I_{y2} are the currents into the two phases of each axis, and R_x and R_y are the

resistances of the coils. The current into the motor has a DC and an AC component:

$$I_{x1} = I_1 + I_2 sin(\omega_x t) \tag{3.6}$$

$$I_{x2} = I_1 + I_2 cos(\omega_x t) \tag{3.7}$$

$$I_{y1} = I_1 + I_2 sin(\omega_y t) \tag{3.8}$$

$$I_{y2} = I_1 + I_2 cos(\omega_y t). \tag{3.9}$$

The AC component is $4A$ and the DC component is $2A$ peak to peak. If the velocities of the two axes are the equal, the frequencies of the sinusoids are then equal:

$$I_{x1} = I_{y1} \tag{3.10}$$

$$I_{x2} = I_{y2}. \tag{3.11}$$

The calculations from this point on assume that if both axes are moving, they are moving at the same velocity. Therefore the motor is moving at a 45° angle to either axis. The experiments conducted met this condition. Substituting equations 3.6 through 3.11 into equation 3.5 yields:

$$q_1 = 4I_1^2 R + K\left(I_2^2 + 2I_1 I_2 sin(\omega t) + 2I_1 I_2 cos(\omega t)\right) R, \tag{3.12}$$

where K equals 0 if neither axis is moving, 1 if one axis is moving or 2 if both axes are moving.

The model considers two heat transfer mechanisms out of the system. Both are forced convection because the motor is moving at all times. Through the bottom and side surfaces, heat leaves the motor and enters the surrounding air. The only convective forces are the air currents caused by the moving motor. The convective heat transfer through the bottom and sides of the motor is given by:

$$q_2 = -\left[h_{bs} A_{bs} (T_m - T_{air})\right], \tag{3.13}$$

where q_2 is the heat transfer rate in watts, h_{bs} is the convection heat transfer coeffi-

cient, A_{bs} is the total surface area of the sides and bottom of the motor, and T_{air} is the ambient air temperature. The value of h ranges from 25 to 250 $\frac{W}{m^2 D}$ for forced convection of gases [5]. The second forced heat transfer term has the same form as the first. The heat transfer through the top of the motor is given by:

$$q_3 = -\left[h_t A_t \left(T_m - T_{air}\right)\right]. \tag{3.14}$$

However, the values of h_t and A_t differ. For the value of h, the motor was assumed to be a flat plate. Using the flat plate correlation gives:

$$\bar{Nu} \equiv \frac{\bar{h}x}{k} = 0.664 Re^{\frac{1}{2}} Pr^{\frac{1}{3}} \tag{3.15}$$

where $\bar{Nu}$ is the Nusselt number, $\bar{h}$ is the average value of h, x is the characteristic length, k is the thermal conductivity of air, Re is the Reynolds number, and Pr is the Prandtl number. Assuming laminar flow allows x to be replaced with L_m, which is the length of the motor. Solving for $\bar{h}$ gives:

$$\bar{h} = \frac{0.664 k Re^{\frac{1}{2}} Pr^{\frac{1}{3}}}{L_m}. \tag{3.16}$$

The theoretical values were calculated using the average heat transfer coefficient, $\bar{h}$. The term that differs between the forced convection through the top and the bottom/sides of the motor is the Reynolds number:

$$Re = \frac{uL}{\nu}, \tag{3.17}$$

where u is the average velocity of the convected air, L is the characteristic length, and ν is the kinematic viscosity of air. The term that differs between top and the bottom/sides is the velocity of the air. The top has the added velocity of the air from the air bearing. For the bottom/sides, the velocity term is given by:

$$u = v_m, \tag{3.18}$$

where v_m is the velocity of the motor. The model assumes that the motor is always traveling at the specified velocity, and ignores the acceleration up to the velocity. For the top, the velocity term is given by:

$$u = v_{bearing} + v_m \tag{3.19}$$

$$= \frac{Q}{A_{flow}} + v_m, \tag{3.20}$$

where Q is the flowrate of the air supplied to the air bearing and A_{flow} is the area of flow for the air bearing (in this case the airgap between the motor and the platen multiplied by the perimeter of the motor).

Equating the energy storage capacity with the heat transfer terms gives the differential equation which describes the temperature behavior of the motor:

$$mc_p \frac{d(T_m - T_{air})}{dt} = q_1 + q_2 + q_3 \tag{3.21}$$

$$= I_1^2 R + K\left(I_2^2 + 2I_1 I_2 sin(\omega t) + 2I_1 I_2 cos(\omega t)\right) R$$

$$- \left[h_{bs} A_{bs} (T_m - T_{air})\right] - \left[h_t A_t (T_m - T_{air})\right]. \tag{3.22}$$

$T_m - T_{air}$ has been substituted for T_m in equation 3.22, because the heat transfer is driving the temperature difference between the motor and its environment. Solving this first order differential equation gives the temperature difference between the air and the motor as a function of time:

$$T_m - T_{air} = \alpha sin(\omega t) + \beta cos(\omega t) + T_f\left(1 - e^{\frac{-t}{\tau}}\right), \tag{3.23}$$

where

$$\alpha = \frac{2I_1 I_2 RK}{mc_p \omega}\left(1 + \frac{h_{bs} A_{bs} + h_t A_t}{mc_p \omega + h_{bs} A_{bs} + h_t A_t}\right) \tag{3.24}$$

$$\beta = -\frac{2I_1 I_2 RK}{mc_p \omega + h_{bs} A_{bs} + h_t A_t} \tag{3.25}$$

$$T_f = \frac{4I_1^2 R + RKI_2^2}{h_{bs} A_{bs} + h_t A_t} \tag{3.26}$$

$$\tau = \frac{mc_p}{h_{bs}A_{bs} + h_t A_t} \tag{3.27}$$

$$\omega = \frac{2\pi v_m}{0.001016}. \tag{3.28}$$

The equation for ω is based on a platen pitch of 0.040" (0.1016 cm). The velocity of the motor is equal to the tooth pitch divided by the period of the current sinusoid, because it takes exactly one cycle to move the force one tooth pitch. From this relationship, ω as a function of v_m can be determined. The velocity of the motor v_m in equation 3.28 has units of $\frac{m}{s}$.

3.1.2 Platen Deformation

Thermal strain results from the heating of the platen. The theory for platen deformation gives an order of magnitude estimate of the thermal strain in the platen. A more sophisticated model would involve finite element modeling of the temperature gradients across the platen. This theory provides a worst-case estimate of the resulting thermal strain. The model incorporates the following assumptions. The platen is assumed to be made of uniform material (steel) rather than etched with polymeric material between the teeth. The second assumption is that the platen reaches a temperature equal to the motor. This consideration is a worst-case scenario. The model assumes that the only area that experiences the thermal strain is the area directly above the motor's area of travel. The model assumes that there is no heat conduction between this area and the surrounding area of the platen. All the heat transfered to the platen remains in the area over which the motor travels. Finally, this analysis uses the final steady state temperature reached by the motor to determine the worst possible strain to the platen.

Thermal strain is expressed as:

$$\epsilon_x = \epsilon_y = \alpha \Delta T, \tag{3.29}$$

where ϵ_x is the strain in the x direction, ϵ_y is the strain in the y direction, α is the coefficient of linear expansion, and ΔT is the temperature change of the material.

The strain is assumed to be uniform in all directions. Therefore the deformations are proportional to the length of the heated region in that direction. If the motor is moving in one direction y, the strains are:

$$\epsilon_y = \frac{\delta_y}{s_{tot}} \tag{3.30}$$

$$\epsilon_x = \frac{\delta_x}{L_m} \tag{3.31}$$

where δ_y and δ_x are the elongations in the y and x directions respectively, s_{tot} is the total commanded displacement of the motor, and L_m is the length of the motor. Substituting equation 3.29 into equations 3.30 and 3.31 and solving for the elongations gives:

$$\delta_y = \alpha \Delta T s_{tot} \tag{3.32}$$

$$\delta_x = \alpha \Delta T L_m. \tag{3.33}$$

If the motor is moving in two directions as illustrated in Figure 3-2, the elongation in the x and y directions are:

$$\epsilon_y = \frac{\delta_y}{L_y} \tag{3.34}$$

$$\epsilon_x = \frac{\delta_x}{L_x}, \tag{3.35}$$

where

$$L_y = L_m + L_m tan(a) \tag{3.36}$$

$$L_x = L_m + \frac{L_m}{tan(a)}. \tag{3.37}$$

Substituting equations 3.36 and 3.37 into equations 3.34 and 3.35 gives the equations for the elongations in x and y:

$$\delta_y = \alpha \Delta T (L_m + L_m tan(a)) \tag{3.38}$$

$$\delta_x = \alpha \Delta T \left(L_m + \frac{L_m}{tan(a)} \right). \tag{3.39}$$

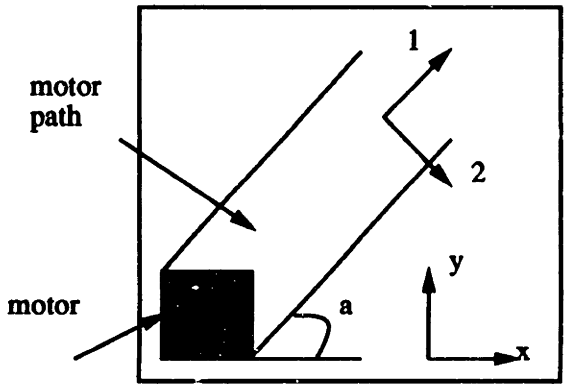

Figure 3-2: Elongations for Motor Travel in X and Y Directions

3.2 Experimental Setup

3.2.1 Experimental Apparatus

Figure 3-3 shows the setup of the thermal experiments. A T-type thermocouple was

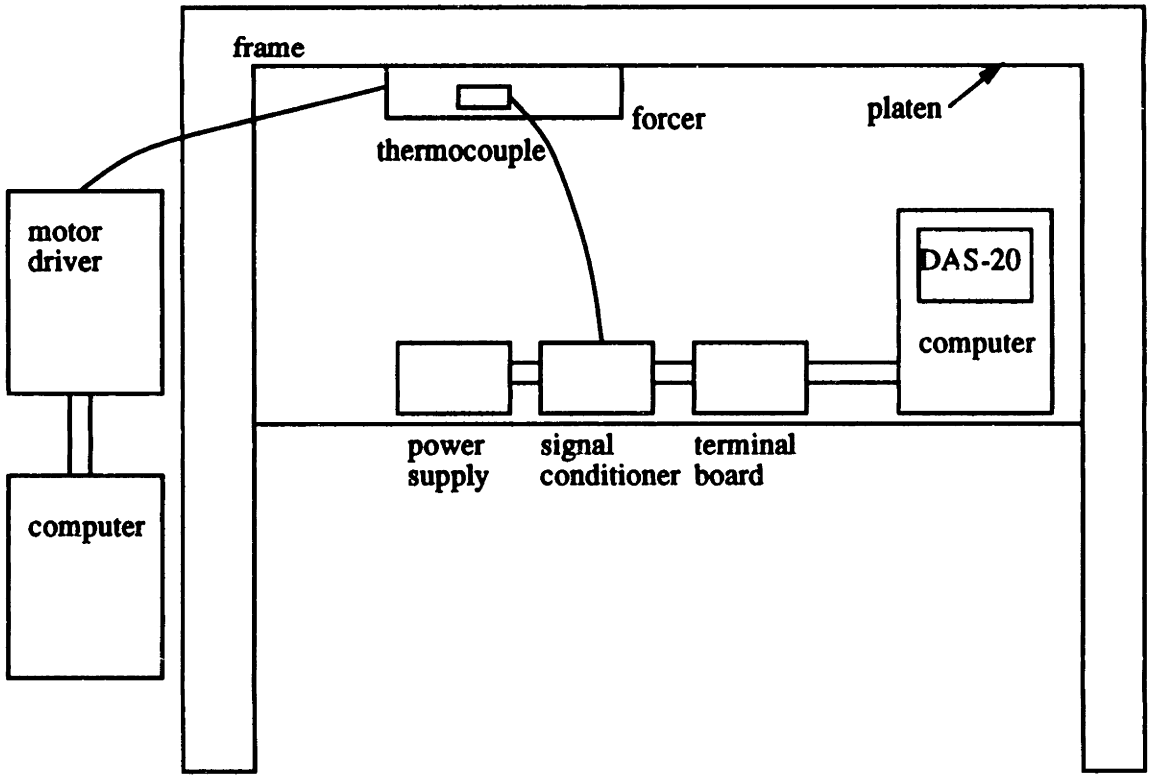

Figure 3-3: Thermal Experimental Apparatus

fastened to the side surface of the linear motor. (See Appendix A for thermocouple description.) The best surface to measure would have been the surface adjacent to the platen. However, it was not feasible to access this surface. T-Type thermocouples were chosen because they have the smallest temperature range. The linear motor is rated to run at $110°C$ maximum. Since the range of the T-type thermocouple is rated up to $250°C$, it was sufficient for the experiment. Choosing a thermocouple with a smaller range also meant greater accuracy since the limits of error are based on the full temperature range of the thermocouple (See Table A.1). The thermocouple used terminated in a flat surface for convenient mounting to the linear motor. A highly conductive tape was used to mount the thermocouples to the surface.

The thermocouple output was linearized by a Metrabyte MB47 signal conditioner.

The signal conditioner also provided cold-junction compensation. A solid-state thermometer sensed the ambient temperature. The output from the signal conditioner was a linear (0 to 5V) voltage corresponding to a temperature range of $0 - 200°C$. The signal conditioner accuracy is also based on the temperature range of the thermocouple type. Therefore, choosing a T-type thermocouple maximized the accuracy of the signal conditioner output. The output from the signal conditioner was connected to a screw terminal board (Metrabyte STA-20). A PC-compatible computer with a 12-bit data acquisition board (Metrabyte DAS-20) collected the output data from the signal conditioner.

3.2.2 Procedure

For each experiment, temperature data was gathered for at least 1 hour. A program written in BASIC (see Appendix B) controlled the sampling period, converted the voltage output from the signal conditioner to a temperature value, and outputed the current temperature to the screen and a file. For the first 2 minutes of each experiment, the program gathered temperature values every second to capture the transient rise of the temperature immediately after turning on the driver. For the remainder of the experiment, the temperature was measured every 15 seconds. For each experiment, the motor was programmed to travel in a straight repetitive path back and forth, over the hour-long time period. (See Appendix B for sample control program using MoPro IIPC software.) The default trapezoidal velocity profile was used for each experiment. Several parameters were varied in each experiment: the velocity, the acceleration, the distance traveled, and the number of axes used. The experiments were performed over a four week period.

3.3 Results and Discussion

3.3.1 Motor Temperature

Transient Temperature Behavior

Table 3.1 shows the various experiments, the parameter values, and the peak temperature reached.

Table 3.1
Thermal Test Settings and Peak Temperatures

Test	Vel. $[\frac{in}{s}]$	Acc. $[\frac{in}{s^2}]$	X $[in]$	Y $[in]$	Peak Temp. $[°C]$
1	0	0	0	0	51.27
2	3.5	100	0	8.0	47.07
3	3.5	100	0	16.0	40.14
4	15	200	0	16.0	49.12
5	15	200	8.0	8.0	59.57
6	24	250	0	16.0	51.17
7	24	250	8.0	8.0	62.50
8	24	250	0	8.0	55.08

Figure 3-4 shows a comparison of experiments whose parameters remained the same except for the distance traveled. Both graphs show experiments conducted using only the y axis. The graph on the left show the temperature traces for velocity

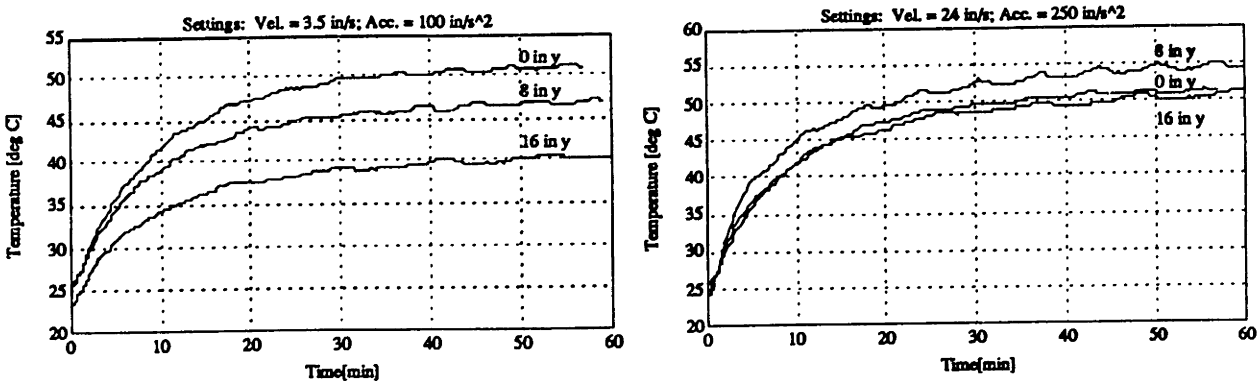

Figure 3-4: Comparison of Motor Temperatures of Various Displacements

of 3.5 $\frac{in}{s}$ (8.89 $\frac{cm}{s}$) and an acceleration of 100 $\frac{in}{s^2}$ (254 $\frac{cm}{s^2}$). The trace on the right

are from experiments conducted at a higher velocity of 24 $\frac{in}{s}$ (60.96 $\frac{cm}{s}$) and higher acceleration of 250 $\frac{in}{s^2}$ (635 $\frac{cm}{s^2}$). The experiment where the motor did not move is shown in both graphs for comparison. At the low velocity and acceleration, the nonmoving experiment reaches the highest temperature. As the distance traveled increases, the peak temperature decreases. As the motor travels further along the platen, more heat is dissipated to the platen and the motor heats up less. At a high velocity the pattern is the same: the longer the distance traveled, the lower the peak temperature. The difference between the high and low velocity curves is that in the high velocity case, the zero velocity curve longer serves as an upper bound for the peak temperature. The 8 *in* (20.32 *cm*) experiment actually reaches a higher peak temperature than the nonmoving experiment.

Figure 3-5 shows two comparisons. The figure on the left show a comparison between changing the velocity of the motor, but leaving the commanded displacement constant. The zero velocity experiment is shown as a reference. As the velocity increases, the peak temperature rises. The graph implies that the zero velocity case is the upper bound for the peak temperature. However, it is possible to infer that increasing the velocity beyond 24 $\frac{in}{s}$ (60.96 $\frac{cm}{s}$) and or increasing the acceleration beyond 250 $\frac{in}{s^2}$ (635 $\frac{cm}{s^2}$) would probably push the peak temperature of the motor over the stationary case.

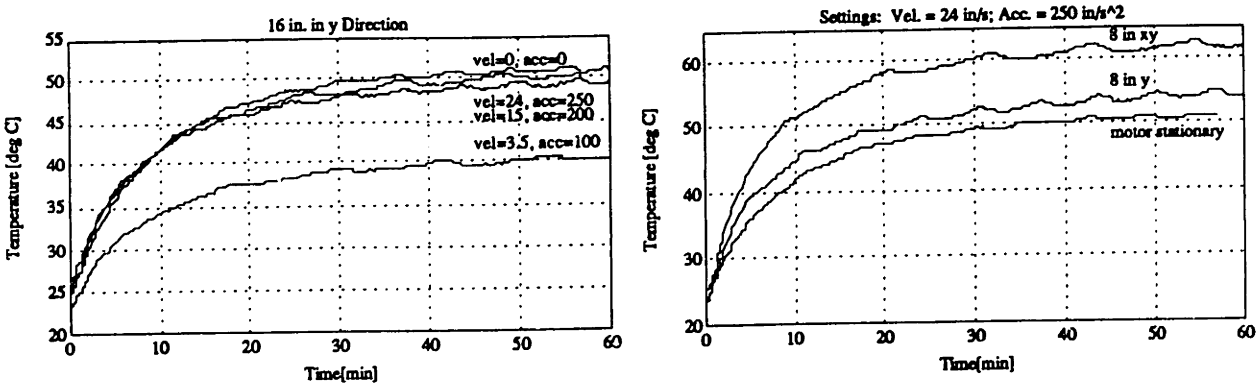

Figure 3-5: Comparison of Motor Temperatures of Various Velocities, Accelerations, and Number of Active Axes

The figure on the right shows a comparison between running neither axis, one axis, and both axes. All other parameters were the same. At the velocity shown in

the figure, even the short displacement (8 in) (20.32 cm)experiment reaches a peak higher than the stationary experiment. When both axes are operating, the motor temperature reaches a higher maximum. In the case where the motor is not moving, there is just a DC current going through the coils. If one axis is moving, an additional AC current flows through half the coils. If both axes are moving, all of the coils see a DC and an AC current.

Comparison With The Theoretical Model

The following values were used for the constants in the theoretical model:

$$m = 2.543kg \tag{3.40}$$

$$L_m = 0.1778m \tag{3.41}$$

$$c_p = 883\frac{J}{kgK} \tag{3.42}$$

$$I_1 = 4A \tag{3.43}$$

$$I_2 = 1A \tag{3.44}$$

$$R = 2\Omega \tag{3.45}$$

$$A_{bs} = 0.05148m^2 \tag{3.46}$$

$$A_t = 0.0316m^2 \tag{3.47}$$

$$k = 0.0263\frac{W}{mL} \tag{3.48}$$

$$\nu = 0.00001589\frac{m^2}{s} \tag{3.49}$$

$$Q = 0.0004719\frac{m^3}{s} \tag{3.50}$$

$$A_{flow} = 0.00001445m^2 \tag{3.51}$$

$$Pr = 0.707 \tag{3.52}$$

The values of v_m, and L changed from experiment to experiment; therefore the values of Re, h, and ω changed from experiment to experiment. Table 3.2 shows the predicted peak change in temperature values for each experiment and the experimental change in temperature.

Table 3.2 Theoretical Peak Temperatures		
Test	Actual Peak Temperature Change [$^{\circ}C$]	Theoretical Peak Temperature Change [$^{\circ}C$]
1	25.4884	76.5517
2	21.3867	66.9469
3	16.4062	47.3386
4	22.6563	43.5173
5	35.2539	58.1984
6	26.0742	41.7483
7	38.7695	48.5993
8	30.9570	59.0410

The predicted peak values are on the order of twice the actual peak temperatures. Therefore, the model is not considering a source of heat loss from the system.

Figures 3-6 through 3-9 show the theoretical model's prediction of the temperature rise of the motor along with the actual experimental results.

In all cases, the model predicted a peak temperature higher than the actual peak temperature. The model showed greater error for the cases where only one axis was moving. For example, the traces in Figure 3-6 show much greater disparity than the left figures in Figure 3-8 and Figure 3-9. This pattern is evidence that the model is more affected by the DC term in the current than the AC term. In the real system, the addition of the AC term has a much greater effect than the model predicts. Figure 3-6 and the left figures in Figures 3-8 and 3-9 confirm this fact. In Figure 3-6 the model overpredicts the peak value by a considerable margin. Neither axis is moving. The model predicts a greater effect due to the DC term than there actually is. When the AC term is added by moving both axes as in Figures 3-8 and 3-9, the experimental "catches up" with the theory. Therefore, AC term (the frequency of the sinusoids) has a larger effect than the DC term. The DC term is always present.

In general, the model also predicted a longer time constant than in the actual system. In most of the cases, the theoretical model takes longer than one hour to reach steady state. In actuality, the most of the experiments reach steady state before an hour.

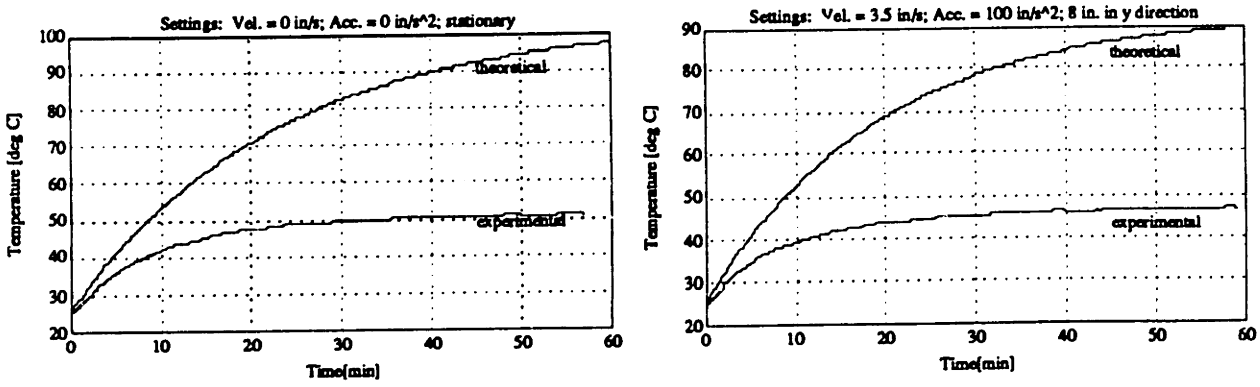

Figure 3-6: Comparison of Theoretical and Experimental Temperature Curves

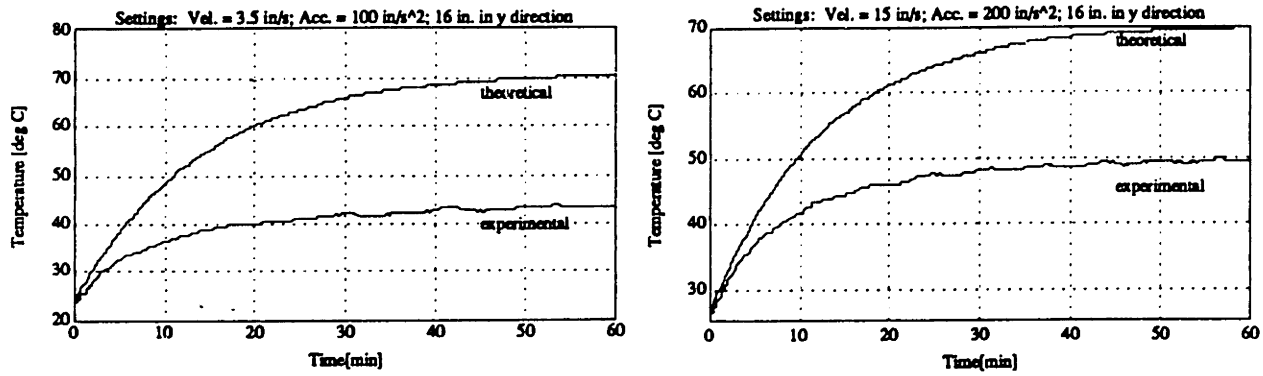

Figure 3-7: Comparison of Theoretical and Experimental Temperature Curves

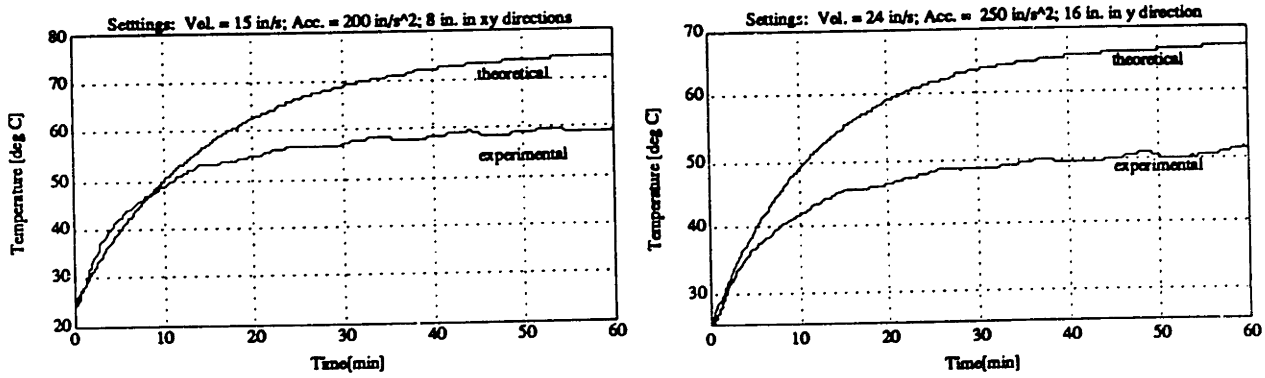

Figure 3-8: Comparison of Theoretical and Experimental Temperature Curves

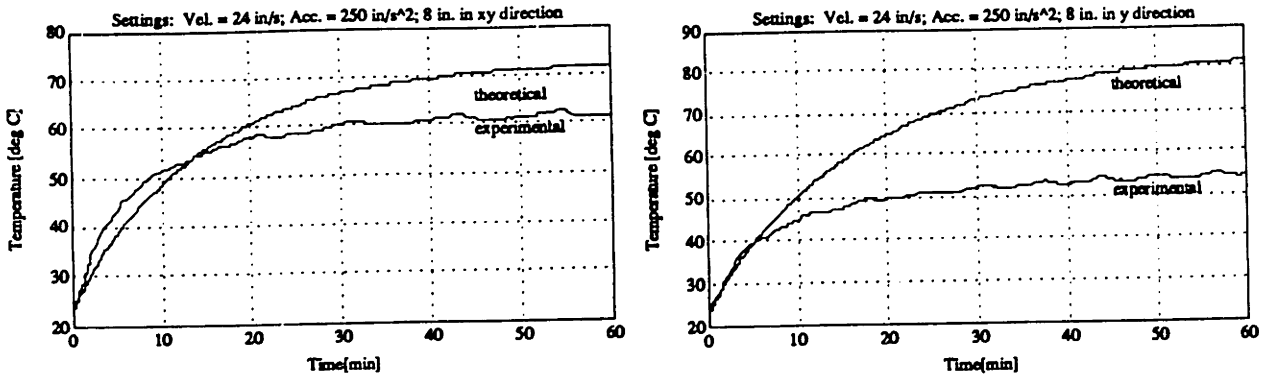

Figure 3-9: Comparison of Theoretical and Experimental Temperature Curves

Several assumptions have made the model inaccurate. The results reveal that the model is not considering some other source of heat loss from the system. The model considered the motor to be a solid block of aluminum. However, there could be heat loss to the air inside the motor. The coils are contained inside a hollow housing. However, it is difficult to assess the conduction to the air inside the motor. Secondly, the motor was assumed to be uniform in temperature. In reality, there exists temperature gradient across the motor from the coils to the outside surface. In ignoring conduction, the model may have neglected a major source of heat loss.

Recalling that the final temperature (equation 3.26) and the time constant (equation 3.27) are both inversely proportional to an hA term, its is likely that this term in the model is too small. Increasing this term would decrease both the final temperature and reduce the time constant of the system. Therefore, the model may have underestimated the forced convection effects on the system. The flat plate correlation may not be sufficient to describe the convection occurring.

Although the model overpredicts the peak temperature, it is still possible to observe trends with respect to changing parameters such as distance traveled, velocity traveled and number of axis in motion. Figure 3-10 shows the experimental and theoretical peak change in temperature versus commanded displacement. All other parameters were kept constant. Both the results from Figure 3-4 are included in Figure 3-10.

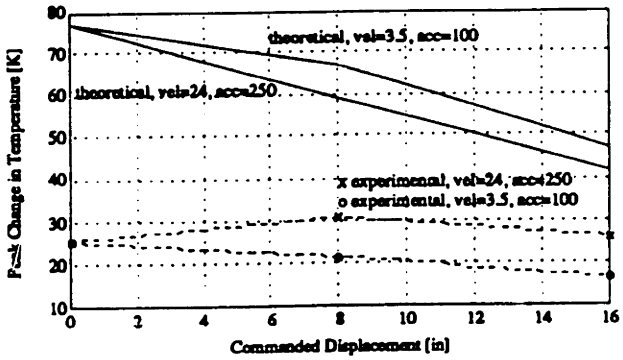

Figure 3-10: Comparison of Peak Temperature Change and Commanded Displacement

The theoretical model states that the peak temperature should decrease with increased commanded displacement. The experimental values follow this pattern. The major discrepancy between the experimental values and the theoretical values is that the theory states that the higher the motor velocity, the lower the peak temperature. Figure 3-10 exhibits this discrepancy. For the theoretical curves, the lower velocity curve is higher. For the experimental curves, the higher velocity curve is higher. Figure 3-11 shows a comparison between the theoretical peak temperature change and the experimental peak temperature change for various commanded velocities.

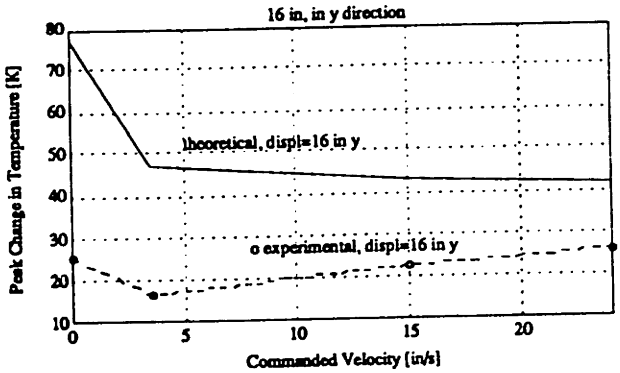

Figure 3-11: Comparison of Peak Temperature Change and Commanded Velocity

In theory, the peak temperature change decreases as velocity increases. In reality, the peak temperature change increases with increased velocity.

The theory exhibits this inverse relationship in two places in the model. The first is in the hA term in the denominator of Equation 3.26. Increasing the velocity of

the motor increases the convection of heat from the motor. (Increasing the velocity increases the denominator of Equation 3.26 which decreases the value of T_p.) The other place this relationship is reinforced in the model is through the frequency of the AC input. The frequency ω of the input sinusoid is proportional to the velocity of the motor. However, since ω is in the denominator of the coefficients α and β, increasing the velocity decreases the values of these coefficient. The model lacks a term which relates an increase in the velocity of the motor (also an increase in the frequency of the AC current) to an increase in heat into the system.

3.3.2 Platen Deformations

Using equations 3.32, 3.33, 3.36 and 3.37, a worst-case prediction for the platen deflection can be determined. Two values for alpha were used:

$$\alpha_1 = 9.9 \times 10^{-6^\circ} C^{-1} \tag{3.53}$$

$$\alpha_2 = 12.8 \times 10^{-6^\circ} C^{-1} \tag{3.54}$$

Typical values of α for steel range from α_1 to α_2. Table 3.3 gives the range of x and y deflections using the experimental peak temperature differences from Table 3.2. Figure 3-12 shows the relationship between the deflections in the platen and

Table 3.3
Platen Deflection

Test	δ_{x1} $[in \times 10^{-3}]$	δ_{x2} $[in \times 10^{-3}]$	δ_{y1} $[in \times 10^{-3}]$	δ_{y2} $[in \times 10^{-3}]$
1	1.766	2.284	1.766	2.284
2	1.482	1.916	1.694	2.190
3	1.137	1.470	2.599	3.360
4	1.570	2.030	3.589	4.640
5	4.886	6.317	4.886	6.317
6	1.807	2.336	4.130	5.340
7	5.373	6.947	5.373	6.947
8	2.145	2.774	2.452	3.170
max	7.733	min	1.137	

the commanded displacement. The figure on the left corresponds to a low veloc-

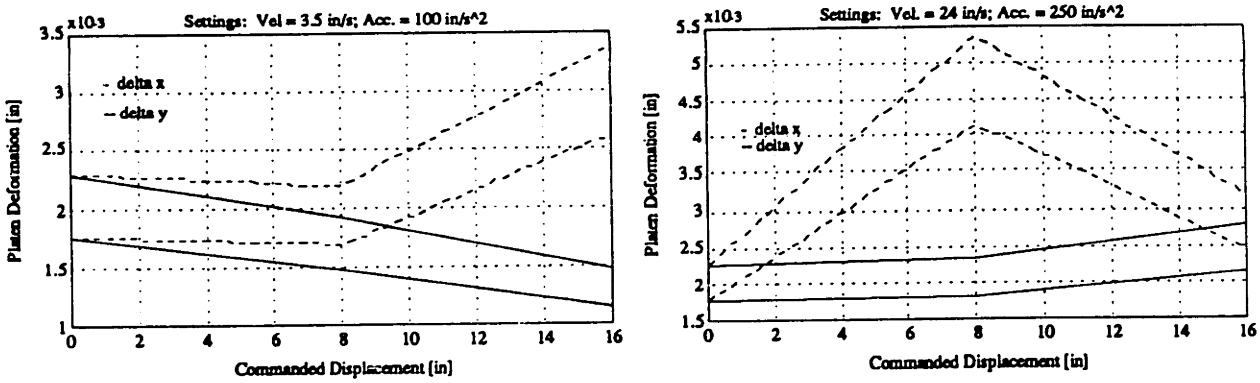

Figure 3-12: Comparison of Platen Deflection and Commanded Displacement

ity and acceleration and the figure on the right corresponds to a high velocity and acceleration. At a slow velocity and acceleration, as the commanded displacement increases, δ_x decreases. The peak temperature decreases, but the length in x remains the same, so a smaller deflection results. In the y direction however, the behavior is drastically different. Initially, an increase in the commanded displacement decreases the deflection. However, as the displacement is increased further, the deflection increases. The peak temperature decreases when the displacement increases. However, the deflection is also a directly proportional the commanded displacement. Since the commanded displacement increases faster than the temperature decreases, a greater deflection results for greater commanded displacements.

The higher velocity in the right figure of Figure 3-12 shows the opposite trend. The decrease in peak temperature from 8 in (20.32 cm) to 16 in (40.64 cm) results in a decrease in the deflection. Although the displacement increases, the decrease in peak temperature has a greater effect, resulting in a smaller deflection.

Figure 3-13 shows the relationship between deflection and commanded velocity and between deflection and number of axes in motion. The left figure in Figure 3-13 shows that increasing the velocity and acceleration of the motor increases the deflection in the direction of travel. The platen not only reaches a higher temperature, but also a greater area of the platen is heated to this temperature. The deflection in the x direction also increases with increased velocity. The area in this direction is

not changing, but the peak temperature change is increasing with increased velocity and acceleration.

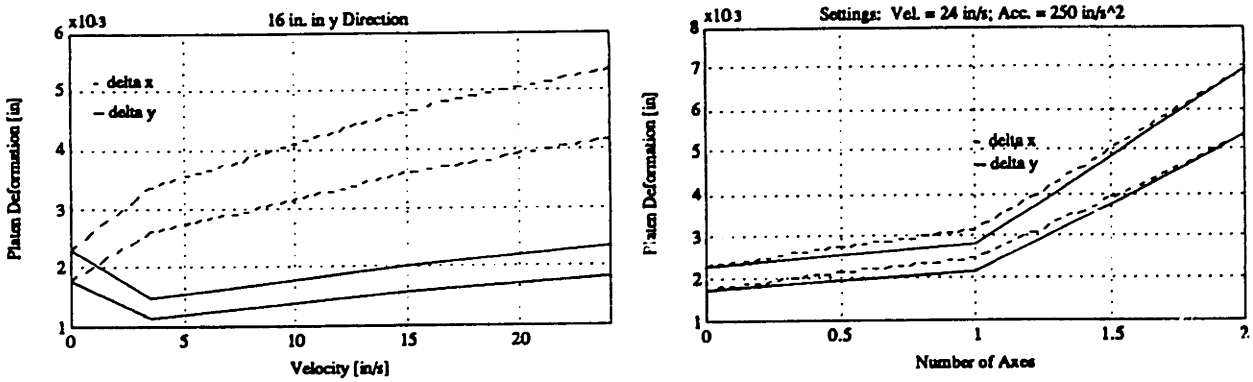

Figure 3-13: Comparison of Platen Deflection of Various Velocities, Accelerations, and Number of Active Axes

The right figure in Figure 3-13 shows that the more axes are used, the greater the deflection. Using both axes heats the platen to a greater temperature.

3.4 Conclusion

The theoretical model verified the first order nature of the heating of the motor. It showed an exponential rise to a steady-state value. It showed the dependence of the temperature behavior on variables such as specified displacement, velocity, acceleration, and the number of active axes.

The values of the deflection range from 2.8% of a tooth pitch to 19.3% of a tooth pitch. For the packaging system being studied, these values seem insignificant. However, these values become significant when considering a system that will be in operation 24 hours a day. A small error may not affect the system performance, but a small repeated error may result in a large error. The errors become significant when considering the implementation of feedback to the system. In the case where the motor loses knowledge of its position, it no longer has the absolute positioning capability of a stepper motor. Thermally induced deflections to the platen may cause these inaccuracies.

A better model should be developed to predict the temperature of the motor. It should include more accurate values for the convective terms. It should consider heat loss by conduction. The model should incorporate the dependence of the heat generated on the velocity of the motor. This model would better predict the temperature of the motor.

Since a worst-case scenario has been established, the next step is to assess in more specific terms the deflections to the platen. The development of a finite element model of the platen would reveal globally the effects of heating the platen. The knowledge of these effects would allow for the development of position knowledge compensation for the motor. The solution would not be simple. The best solution is to eliminate the heat before it reaches the platen. A system to cool the motor as it runs would decrease the heat transferred to the platen, and therefore the deflections. Perhaps the air bearing could be better used to assist in cooling the motor. These actions would lead to maintaining the accuracy of the linear motor.

Chapter 4

Motion Control

4.1 Background

In the linear motor, motion is generated by inputing two current sine waves 90° out of phase to each of the electromagnetic coils. The frequency of the sine waves determine the velocity. The rate of change of frequency determines the acceleration. The leading sinusoid determines the direction of travel. The resolution of the position of the motor is determined by a combination of the pitch of the platen teeth and the microstepping ability of the driver. In the system studied, the pitch was 0.040" (0.1016 cm) and the microstepping capability was 4 to 125 microstep per full step. One cardinal step being one-quarter the tooth pitch makes the finest resolution of the motor 0.010" (0.0254 cm) divided by 125 or 0.08 thousandths of an inch (203.2 μm).

As described in Chapter 2, the linear motor was driven by a Motion Science Micro Step Motor Drive. The controller was a Motion Science MoPro IIPC Board. A Control program included with the board allowed interfacing with the controller board, and the development of motion control programs.

The MoPro IIPC performs three types of motion. Point to Point positioning allows specification of a position to which the motor will move . It requires specification of a velocity, acceleration and a velocity profile. Continuous motion positioning allows commands of constant or changing velocity without specifying position. It is useful for applications which do not require position information, and only require velocity

information. The final type of motion is Seek positioning, which allows the motor to move until a physical reference is located.

All of the experiments were conducted using Point to Point positioning. Point to Point positioning may be performed by either axes independently or both axes simultaneously. The default velocity profile is a trapezoidal profile. Figure 4-1 shows a typical move using the trapezoidal velocity profile. A certain position, velocity, and acceleration have been specified to the controller. During the time period T_1, the

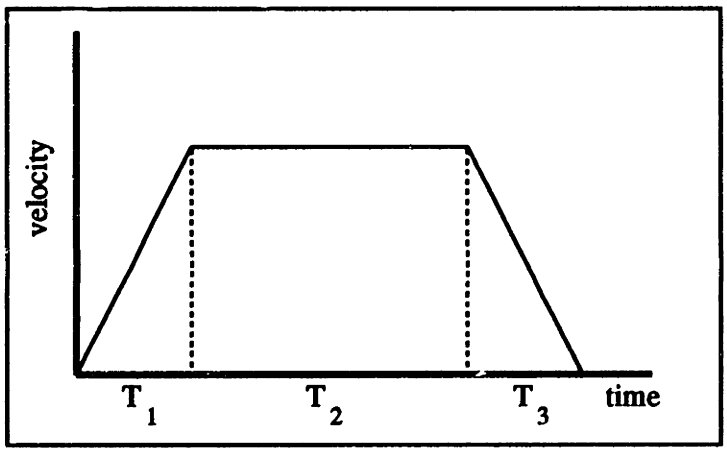

Figure 4-1: Trapezoidal Velocity Profile

motor will accelerate at the rate specified. During T_2, it has reached the specified velocity, and will maintain a constant velocity. During T_3, the motor decelerates down to zero velocity, stopping at the commanded position. MoPro IIPC calculates the time required to accelerate to the specified velocity and sets T_1 equals T_3. Then it calculates how long to run at the top velocity T_2, such that the motor will decelerate and stop at the commanded position.

Since the acceleration is constant, during T_1 the velocity V is given by:

$$v = a_s t, \tag{4.1}$$

where a_s is the acceleration specified and t is the time. To determine T_2, T_1 and T_3 must be calculated. The time to accelerate and decelerate is found by solving for t in

equation 4.1 and substituting V_p, the specified peak velocity:

$$T_1 = T_3 = \frac{V_p}{a_s}. \tag{4.2}$$

The distance traveled during acceleration and deceleration is given by:

$$s_1 = s_2 = \frac{1}{2} a_s T_1^2, \tag{4.3}$$

where s_1 and s_2 are the displacements during T_1 and T_2 respectively. The distance s_2 traveled during T_2 is given by:

$$\begin{aligned} s_2 &= s_{tot} - s_1 - s_2 && (4.4) \\ &= s_{tot} - a_s T_1^2, && (4.5) \end{aligned}$$

where s_{tot} is the specified distance to travel. Finally, T_2 is given by

$$\begin{aligned} T_2 &= \frac{s_2}{V_p} && (4.6) \\ &= \frac{s_{tot} - a_s T_1^2}{V_p} && (4.7) \\ &= \frac{s_{tot}}{V_p} - \frac{V_p}{a_s} && (4.8) \end{aligned}$$

Table 4.1 summarizes the motor motion for a trapezoidal velocity profile.

Table 4.1
Trapezoidal Profile Characteristics

	T_1	T_2	T_3
duration	$\frac{V_p}{a_s}$	$\frac{s_{tot}}{V_p} - \frac{V_p}{a_s}$	$\frac{V_p}{a_s}$
displacement	$\frac{1}{2} a_s t^2$	$-\frac{V_p^2}{2a_s} + V_p t$	$\frac{a_s s_{tot}^2}{2V_p^2} - \frac{V_p^2}{2a_s} + V_p t + \frac{a_s s_{tot}}{V_p} t - \frac{1}{2} a_s t^2$
velocity	$a_s t$	V_p	$V_p + \frac{a_s s_{tot}}{V_p} - a_s t$
acceleration	a_s	0	$-a_s$

If the position commanded prescribes a short move that does not allow the axis

to reach the specified velocity, a triangular velocity profile results. The condition for a triangular profile to occur is as follows (derived in Appendix C):

$$s_{tot} < \frac{V_p^2}{a_s}. \tag{4.9}$$

Figure 4.3 shows a triangular velocity profile. The motor accelerates for half the

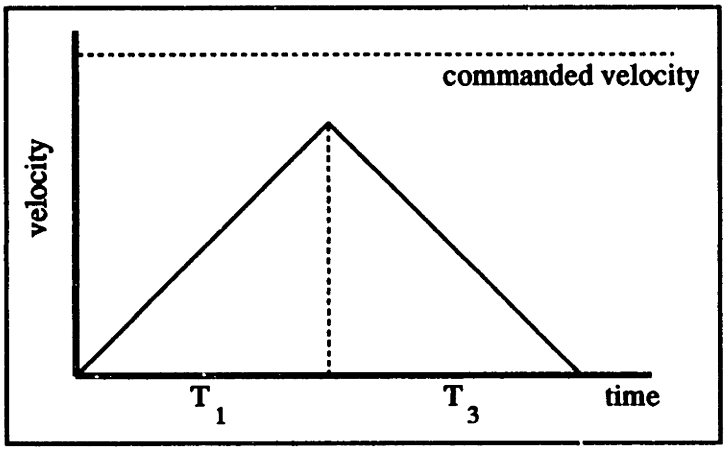

Figure 4-2: Triangular Velocity Profile

distance commanded and decelerates for the remaining half. It never reaches the commanded velocity.

Equation 4.3 also holds for the triangular velocity profile. Substituting in half the total commanded distance for the displacement gives

$$\frac{s_{tot}}{2} = \frac{1}{2} a_s T_1^2. \tag{4.10}$$

Solving for T_1 gives

$$T_1 = T_3 = \sqrt{\frac{s_{tot}}{a_s}}. \tag{4.11}$$

Table 4.2 summarizes the motor motion for a triangular velocity profile.

Table 4.2 Triangular Profile Characteristics		
	T_1	T_3
duration	$\sqrt{\frac{s_{tot}}{a_s}}$	$\sqrt{\frac{s_{tot}}{a_s}}$
displacement	$\frac{1}{2}a_s t^2$	$s_{tot} - \sqrt{\frac{s_{tot}}{a_s}}V_p + V_p t + a_s\sqrt{\frac{s_{tot}}{a_s}}t - \frac{1}{2}a_s t^2$
velocity	$a_s t$	$V_p + a_s\sqrt{\frac{s_{tot}}{a_s}} - a_s t$
acceleration	a_s	$-a_s$

Implementing a smooth velocity profile makes better use of the motor's acceleration characteristics than a constant acceleration profile. It provides high acceleration at low speeds and decreasing acceleration at higher speeds. The motor's initial acceleration is high and decreases to zero as it reaches the commanded velocity. Figure 4.3 shows a smooth velocity profile.

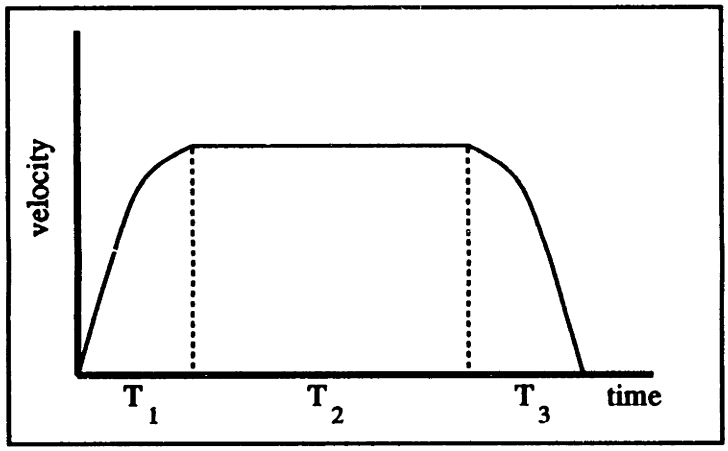

Figure 4-3: Smooth Velocity Profile

The velocity during T_1 follows a parabola given by the following equation (see Appendix C for derivation):

$$V = -\left(\frac{a_s^2}{4V_p}\right)t^2 + a_s t. \tag{4.12}$$

During T_2, the velocity is constant at the specified V_p. During T_3, the velocity follows

the same parabola specified by equation 4.12 shifted by T_2:

$$V = -\left(\frac{a_s^2}{4V_p}\right)(t - T_2)^2 + a_s(t - T_2). \tag{4.13}$$

Table 4.3 summarizes the motor motion for a smooth velocity profile. See Appendix C for the derivations of these expressions.

Table 4.3
Smooth Profile Characteristics

	T_1	T_2	T_3
duration	$\frac{2V_p}{a_s}$	$\frac{s_{tot}}{V_p} - \frac{8V_p}{3a_s}$	$\frac{2V_p}{a_s}$
displacement	$-\left(\frac{a_s^2}{12V_p}\right)t^3 + \frac{1}{2}a_s t^2$	$\frac{2V_p^2}{3a_s} + V_p t$	$-\left(\frac{a_s^2}{12V_p}\right)\left(t - \frac{s_{tot}}{V_p} + \frac{8V_p}{3a_s}\right)^3 + \frac{1}{2}a_s\left(t - \frac{s_{tot}}{V_p} + \frac{8V_p}{3a_s}\right)^2$
velocity	$-\left(\frac{a_s^2}{4V_p}\right)t^2 + a_s t$	V_p	$-\left(\frac{a_s^2}{4V_p}\right)\left(t - \frac{s_{tot}}{V_p} + \frac{8V_p}{3a_s}\right)^2 + a_s\left(t - \frac{s_{tot}}{V_p} + \frac{8V_p}{3a_s}\right)$
acceleration	$-\left(\frac{a_s^2}{2V_p}\right)t + a_s$	0	$-\left(\frac{a_s^2}{2V_p}\right)\left(t - \frac{s_{tot}}{V_p} + \frac{8V_p}{3a_s}\right) + a_s$

The parabolic velocity profile is analogous to the triangular velocity profile. If the distance commanded is too short, the motor will never reach the commanded velocity. The result is a parabolic velocity profile. The condition for a parabolic profile to occurs is as follows (derived in Appendix C):

$$s_m < \frac{16V_p^2}{3a_s}. \tag{4.14}$$

A parabolic profile is shown in Figure 4-4. The MoPro IIPC software fits a parabola to three points. The first curve fit point is the initial point 0,0. The second point is determined by following the parabolic trajectory suggested by the initial acceleration. The peak velocity reached by the motor is less than the actual specified peak velocity. The actual peak velocity is the velocity on the parabolic trajectory when the motor has moved half the specified distance. To determine the third curve fit point, the trajectory of the same parabola shifted must be considered. The third point is the

point where the shifted parabola crosses the t axis (zero velocity).

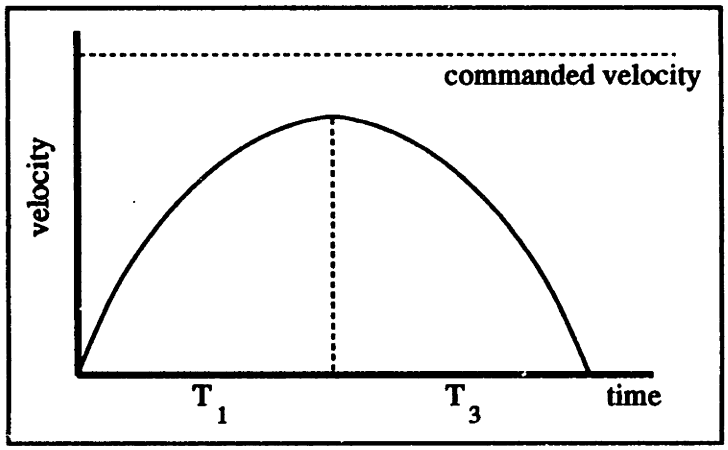

Figure 4-4: Parabolic Velocity Profile

The resulting equation for the velocity (derived in Appendix C) is given by:

$$V = \left(\frac{\sqrt{6}a_s^{1.5}}{6\sqrt{s_{tot}}}\right) t^2 + a_s t. \tag{4.15}$$

Table 4.4 summarizes the motor motion for a parabolic velocity profile. The expressions are derived in Appendix C.

Table 4.4
Parabolic Profile Characteristics

	T_1	T_3
duration	$\frac{1}{2}\sqrt{\frac{6s_{tot}}{a_s}}$	$\frac{1}{2}\sqrt{\frac{6s_{tot}}{a_s}}$
displacement	$\left(\frac{\sqrt{6}a_s^{1.5}}{18\sqrt{s_{tot}}}\right) t^3 + a_s t^2$	$\left(\frac{\sqrt{6}a_s^{1.5}}{18\sqrt{s_{tot}}}\right) t^3 + a_s t^2$
velocity	$\left(\frac{\sqrt{6}a_s^{1.5}}{6\sqrt{s_{tot}}}\right) t^2 + a_s t$	$\left(\frac{\sqrt{6}a_s^{1.5}}{6\sqrt{s_{tot}}}\right) t^2 + a_s t$
acceleration	$\left(\frac{\sqrt{6}a_s^{1.5}}{3\sqrt{s_{tot}}}\right) t + a_s$	$\left(\frac{\sqrt{6}a_s^{1.5}}{3\sqrt{s_{tot}}}\right) t + a_s$

Both axes can be moved simultaneously. The MoPro IIPC commands the axes to start and stop simultaneously. The trajectory for two-axis motion will be a straight line between any two points. If both axes are commanded to move the same distance, then they will have the same velocity profile. If the distances are different then the

velocity profiles must be different to insure that both axes arrive at the commanded position at the same time. Figure 4-5 shows the velocity profiles of a command where the x axis travels twice as far as the y axis. In this case, MoPro IIPC assigns the axis

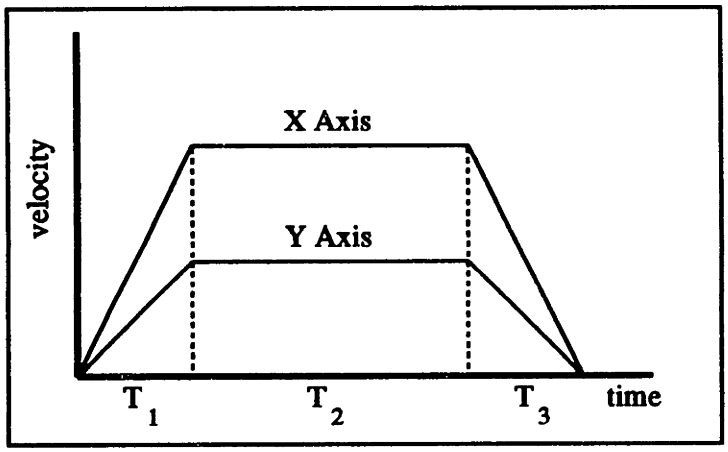

Figure 4-5: Coordinated Velocity Profile

with the longer distance as the Major axis. It uses the velocity and acceleration values specified for this axis to determine the velocity profile. Then it ratios the velocity and accelerations of the other axis (the Minor axis) such that both axes arrive at the commanded position at the same time. In Figure 4-5, because the x axis has to travel twice as far, it is always moving at twice the velocity of the y axis. For the experiments in this study, all the motions were in the y axis. Therefore, coordinated motion was not implemented.

4.2 Experimental Setup

4.2.1 Experimental Apparatus

Figure 4-6 shows the setup of the motion control experiments. A Lucas Schaevitz

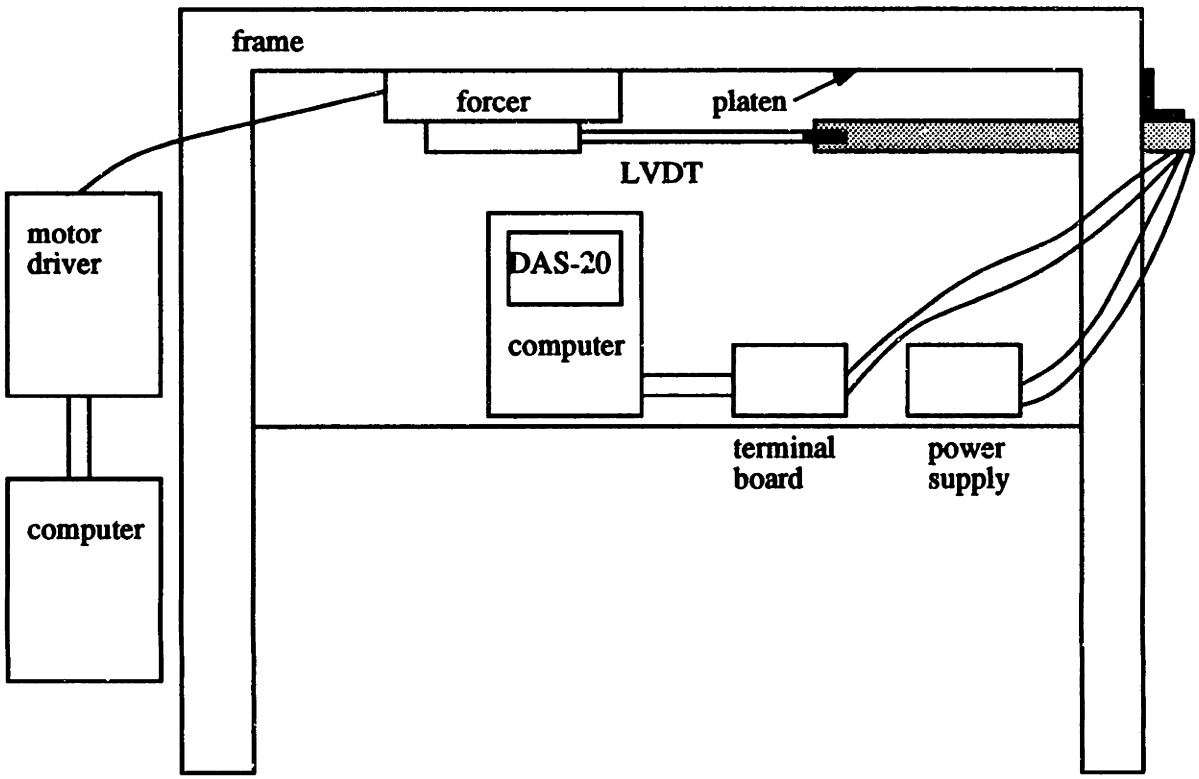

Figure 4-6: Motion Control Experimental Apparatus

Model DCE2000 linear variable differential transducer (LVDT) measured the absolute position of the linear motor in the y direction. It had a full sensing range of 20" (50.8 *cm*). See Appendix D for a description of the LVDT. The core of the LVDT was attached to a plate under the linear motor via a threaded extension rod. The housing of the LVDT was fixtured to the frame of the platen. All of the experiments were held fixing the x axis of the linear motor constant. A $\pm 12V$ power supply powered the LVDT.

The LVDT output was a linear $\pm 10V$ corresponding to a displacement of $\pm 10''$ (± 25.4 *cm*). The LVDT had a specified linearity rating of 0.25% of its full range. The output from the LVDT connected to the Metrabyte STA-20 screw terminal board. The same PC-compatible computer and data acquisition board used in the thermal

experiments collected the output data from the LVDT.

4.2.2 Procedure

The motion control experiments implemented four different velocity profiles: trapezoidal, triangular, smooth, and parabolic. For each profile, velocities, accelerations, distance traveled and loads were varied. The x coordinate of the motor was fixed. Programs written using the Control software included with the MoPro IIPC commanded the motor to move in the y direction only. (See Appendix E for sample control programs using MoPro IIPC software.) A program written in BASIC (see Appendix E) controlled the sampling period, converted the output voltage from the LVDT to a position value, and outputed the position to the screen and a file. The output of the LVDT was sampled at a rate of 800 hz. The position data was numerically differentiated using MATLAB to give velocity and acceleration profiles. The output of the LVDT was had little noise (25 *millivolt* RMS ripple) in the output. In order to eliminate differentiation problems, the position information was averaged every 40 values before differentiated.

4.3 Results and Discussion

Table 4.5 summarizes the experiments conducted. All four velocity profiles were implemented. [1]

Table 4.5
Motion Control Experiments

Experiment	s_{tot} $[in]$	V_p $[\frac{in}{s}]$	a_s $[\frac{in}{s^2}]$	profile	load [lb]
1	8	15	50	trapezoidal	0
2	8	15	10	triangular	0
3	8	15	50	parabolic	0
4	8	15	10	parabolic	0
5	8	15	200	smooth	0
6	15	40	250	trapezoidal	0
7	15	40	100	triangular	0
8	15	40	100	parabolic	0
9	15	40	250	parabolic	0
10	15	40	600	smooth	0
11	8	15	50	trapezoidal	5
12	8	15	10	triangular	5
13	8	15	200	smooth	5
14	8	15	50	parabolic	5

4.3.1 Position and Velocity Profiles

The default signal generates a trapezoidal velocity profile. Figure 4-7 shows the motor position versus time and the motor velocity versus time. The motor reached the peak velocity of 40 $\frac{in}{s}$ (101.6 $\frac{cm}{s}$). The trapezoid shows the theoretical velocity profile according to Table 4.1. The crosses indicate the actual average motor velocity at that time.

[1] Not all of the experiments conducted are discussed in this section. Several experiments of interest are discussed and the results of the remaining experiments can be found in Appendix F.

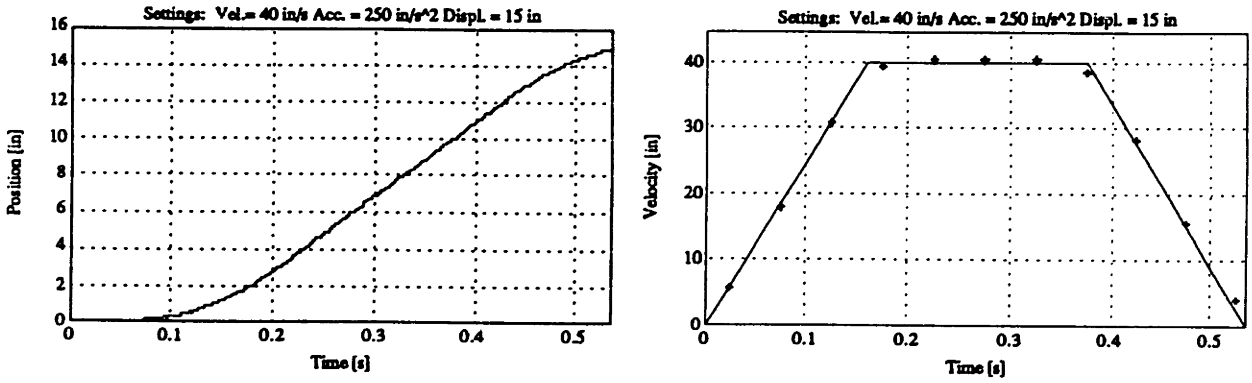

Figure 4-7: Trapezoidal Velocity Profile

The actual motor performance has good agreement with the theory. The two points at the edges of the flat part of the curve are less than the theory. The discrepancy is due to averaging errors for the velocity. The actual peak velocity is also higher than the theoretical.

In the case where the specified distance does not allow the motor to accelerate to the peak velocity, a triangular velocity profile results. Figure 4-8 shows the position and profile for an input velocity of 40 $\frac{in}{s}$ (101.6 $\frac{cm}{s}$) and an acceleration of 100 $\frac{in}{s^2}$ (254 $\frac{cm}{s^2}$). The specified distance 15 in (38.1 cm) does not meet the requirement for a trapezoidal velocity profile. The motor accelerates for the first half the specified distance and decelerates for the second half. Again, the motor meets the theoretical

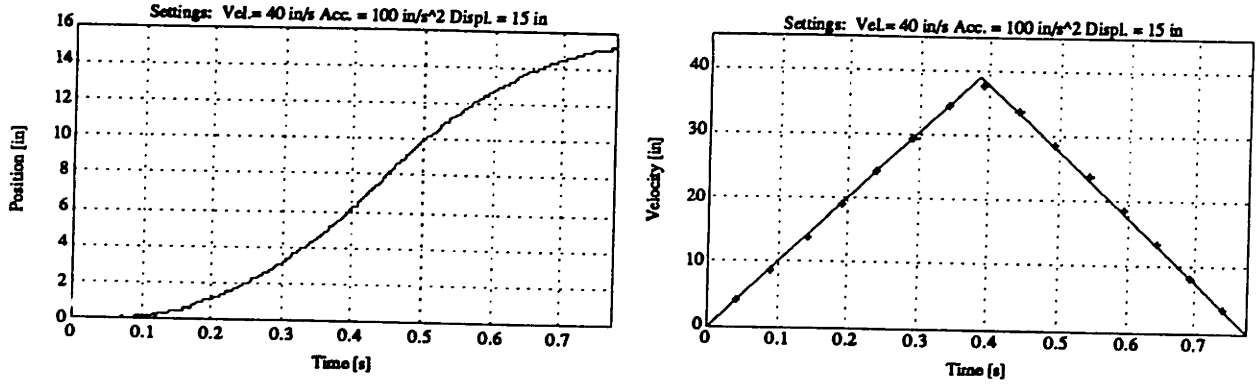

Figure 4-8: Triangular Velocity Profile

curve.

Figure 4-9 shows the position and velocity curve for a smooth velocity profile. The drive specified a peak velocity of 40 $\frac{in}{s}$ (101.6 $\frac{cm}{s}$) and an initial acceleration of 600

$\frac{in}{s^2}$ (1524 $\frac{cm}{s^2}$). The specified displacement of 15 in (38.1 cm) gave the motor space to accelerate to the peak velocity. As in the trapezoidal velocity profile, the actual peak

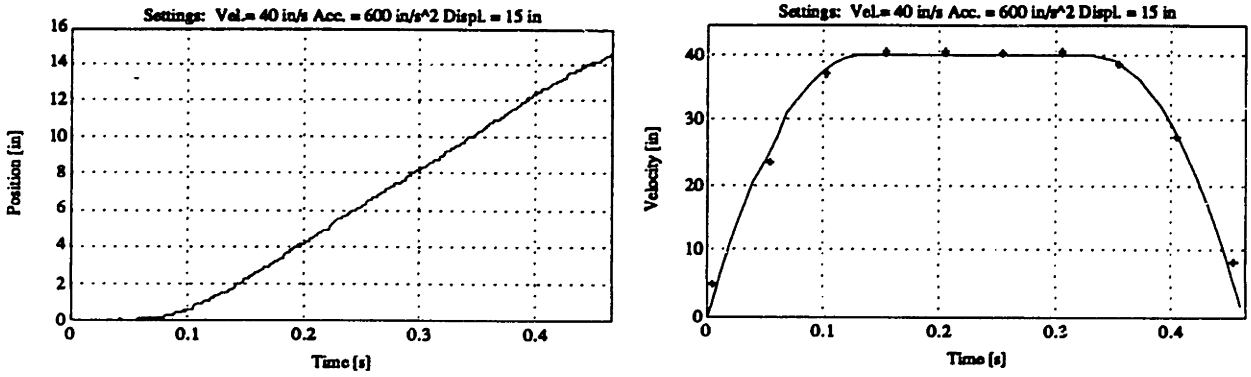

Figure 4-9: Smooth Velocity Profile

velocity is higher than the theoretical.

If the initial acceleration is decreased, the motor cannot accelerate to the peak velocity. Figure 4-10 shows the position and velocity profile for an initial acceleration of 250 $\frac{in}{s^2}$ (635 $\frac{cm}{s^2}$). The motor follows the curve except at points near the peak

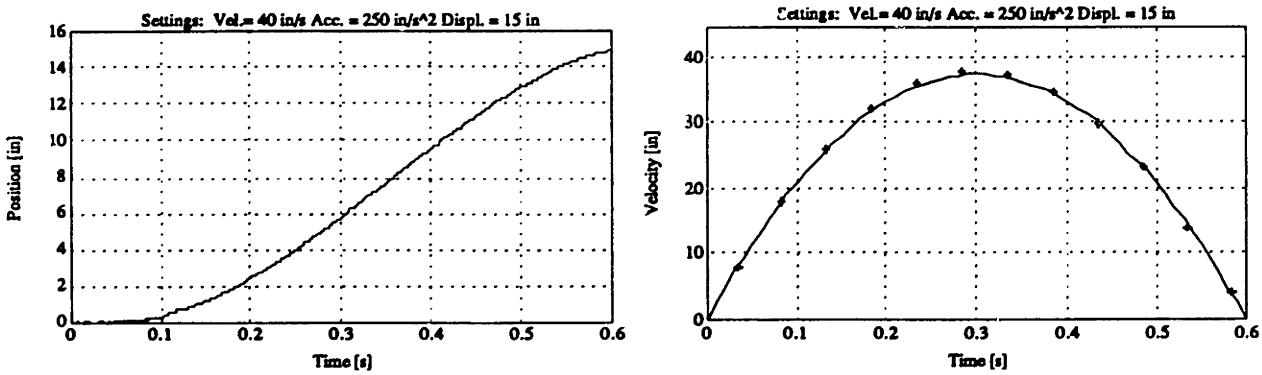

Figure 4-10: Parabolic Velocity Profile

velocity.

4.3.2 Comparison of No Load Versus Loaded Velocity Profiles

The effect of adding a 5 lb (22.24 N) load to the motor did not affect its positioning accuracy. Figure 4-11 shows the velocity profiles for trapezoidal and triangular veloc-

ity profiles. (See Appendix F for position versus time plots.) Adding the 5 *lb* (22.24

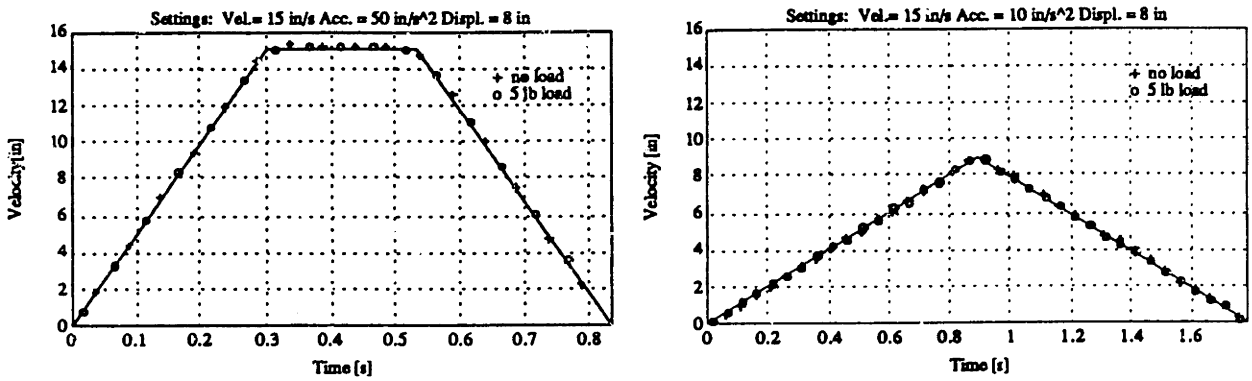

Figure 4-11: Constant Acceleration: Comparison of No Load Versus Load

N) load to the motor did not decrease its positioning accuracy.

Figure 4-12 shows the velocity profiles for the smooth and parabolic velocity profiles. The graphs follow the same trends as the corresponding ones from the previous

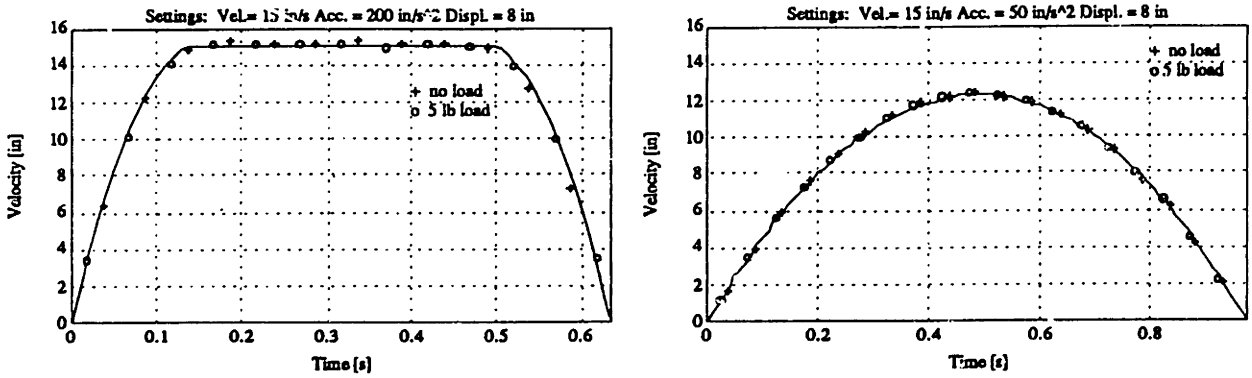

Figure 4-12: Linear Acceleration: Comparison of No Load Versus Load

section. The motor follows the curves except near the peak velocity. At the peak velocity, the motor velocity exceeds the theoretical.

4.4 Conclusion

The positioning ability of the motor is accurate. It has the ability to follow the specified velocity profile even when loaded. It was observed that if the motor had the capability to move a load, it would do so accurately. If the load were to large, or the acceleration too high, the motor would simply stall. It would not perform the commanded move at a lower acceleration or velocity.

The motor was limited in the acceleration it could reach when operating in the default trapezoidal mode. The force required to accelerate quickly at high velocities is more than the motor can output. Implementing the smooth and parabolic profiles allowed the motor to start at a greater acceleration and lower velocity. The motor has no problem with attaining high accelerations at low velocities. The smooth and parabolic trajectories gave the best performance in terms of time. The same move could be performed in less time by implementing these velocity profiles.

Chapter 5

Conclusion

This thesis investigated linear motor performance in two areas. Temperature tests assessed the effects of heat dissipation. Implementation of trapezoidal, triangular, smooth and parabolic velocity profiles determined the positioning accuracy of the motor.

Measuring the temperature of the motor as a function of time revealed the first order thermal behavior of the motor. The motor temperature experiences an exponential rise up to a steady state peak temperature. The peak temperature is affected by several motor parameters. Increasing the velocity of the motor increases the peak temperature. Increasing the specified distance traveled by the motor decreases the peak temperature of the motor.

These patterns have implications on what parameter values to use. The concern is greater if the motor is to be in continuous use. If a high throughput rate is required, a high velocity and a small displacement are desired. However, choosing these two extremes will have double the effect on the peak temperature.

The implications of running the linear motor at a higher temperature are greater deformations to the platen. Running at higher temperatures causes greater thermal strain in the platen. The experiments and the thermal strain model revealed worst-case platen deflections of $\frac{1}{5}$ of a tooth pitch. This amount of deflection does not seem significant if high tolerances are not required. However, should the motor lose knowledge of its position by this amount 5 times, it will be incorrect in its positioning

by an entire tooth pitch.

The most straightforward way to alleviate these complications is to design a way to reduce motor heating. If there is a way to keep motor temperature down, less heat will transfer to the platen. Another solution is to design optimal paths along the platen for the motor. Optimal paths may include not only geometrical specifications along the platen, but also motor parameter specifications. Specific velocity profiles, velocity and acceleration values, and microstepping may be specified.

The thermal effects affect the positioning accuracy of the motor, the second topic of this thesis.

Position testing revealed the ability of the motor to follow specific velocity profiles. Adding a 5 lb (22.24 N) load at low velocities did not affect its positioning accuracy. However, larger loads and higher velocities were not tested.

Implementing different velocity profiles showed that the motor was able to move equal distances faster when using smooth or parabolic profiles. The motor was able to accelerate to a higher velocity because it could start out with a high acceleration at low velocity. Then as the motor increased its velocity, the acceleration decreased.

In order to attain higher velocities and accelerations, it is necessary to understand the current limitations of the motor. The velocity profile that is most efficient (a combination of requiring less time and less motor force) may cause a higher peak temperature resulting in platen deformations. There is a trade-off between the two. Understanding the thermal characteristics of the motor and its effects to the platen will lead to a better understanding of how to make the motor faster and more reliable. Understanding the characteristics of each velocity profile and the motor's performance with respect to each will lead to correctly choosing which to implement for each application. The future of linear motors may include the feedback of position and velocity to control the motor close-loop. However, first there needs to be an understanding of the current capabilities of the linear motor.

Appendix A

Thermocouples

A thermocouple consists of a junction of two dissimilar homogeneous metals. It's principle of operation is based on the Seebeck effect, discovered by Thomas Seebeck in 1821. The Seebeck effect states that when two dissimilar metals are joined at both ends, and the two ends are at different temperatures, a current flows in this thermoelectric circuit. See Figure A-1. The current flows from the hotter junction (T_2) to the colder junction (T_1) through the positive metal (Metal A).

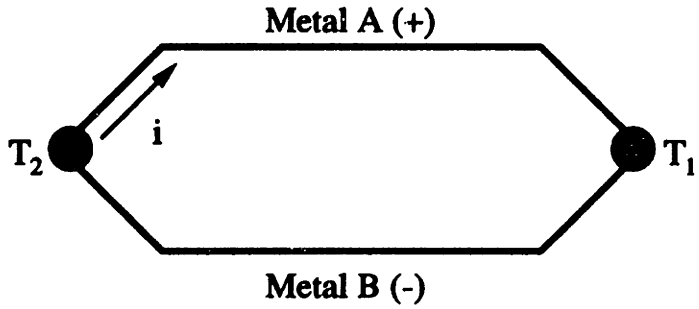

Figure A-1: Seebeck Effect

If the circuit pictured in Figure A-1 is broken, the Seebeck voltage can be measured. This voltage is a function of the temperature difference between what is termed the sensing, or hot-end junction and a reference junction. This voltage also depends on the temperature level and the materials of the thermocouple. The thermocouple

circuit is shown in Figure A-2.

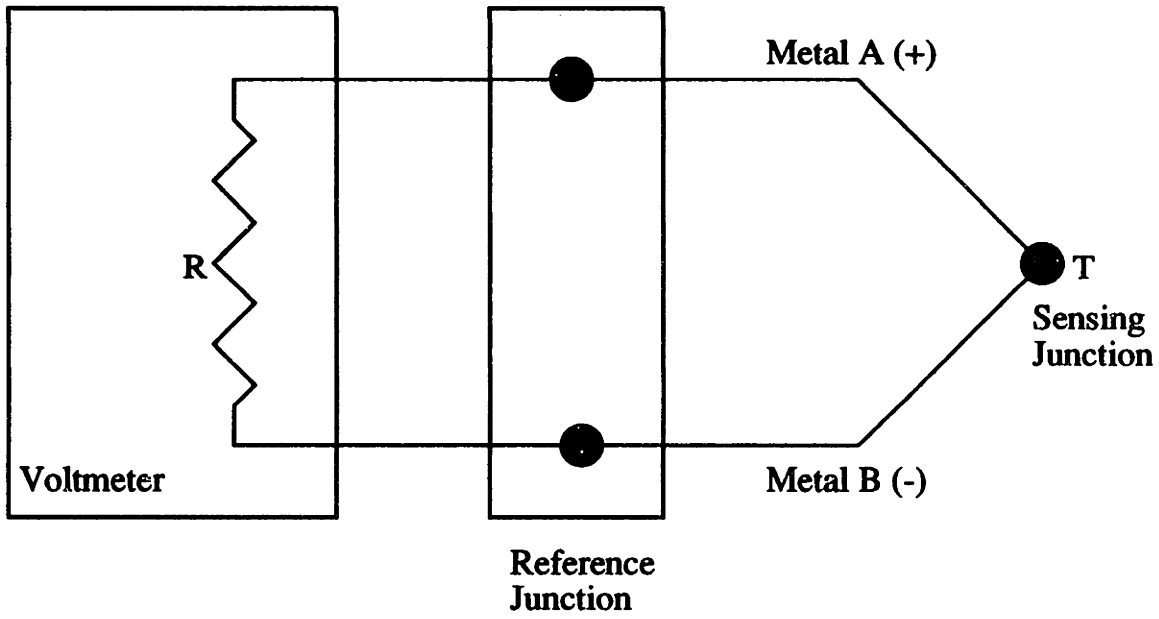

Figure A-2: Thermocouple Circuit

In most cases, the leads from the thermocouple are not long enough to reach the data system. Thermocouple extension wire is used to connect the thermocouple to the instrumentation. See Figure A-3. The extension leads are manufactured to duplicate the thermocouple's voltage-temperature behavior, in effect lengthening the thermocouple leads.

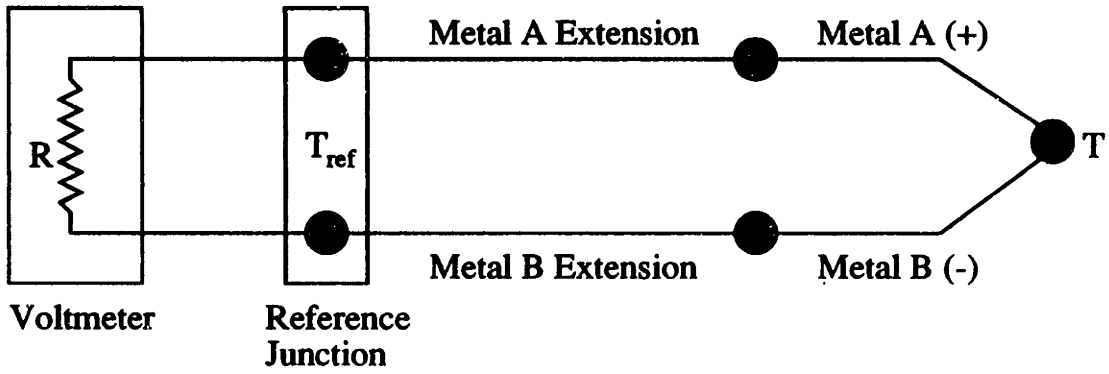

Figure A-3: Thermocouple Extension Circuit

For most pairs of metals, the output voltage e is not a linear function of the temperature. However for small changes in temperature, the Seebeck voltage can be

approximated by:

$$e = \alpha T, \tag{A.1}$$

where α is the Seebeck coefficient for a particular pair of metals, and T is the temperature difference. Thermocouple calibration tables based on a reference junction temperature of $0°C$ exist for standard thermocouples and are called thermocouple tables. In actual practice, the reference junction need not be at $0°C$.

There exist two ways to calculate the absolute temperature of the sensing junctions: hardware or software compensation. Hardware compensation involves either fixing the reference junction at a particular temperature or compensating for the voltage created by the (reference junction) ambient environmental temperature. A logical reference would be to fix the temperature at $0°C$ or to compensate for it's respective voltage. Then the temperature can be read directly from the standard thermocouple table referenced from $0°C$.

The classical way of performing hardware compensation is by keeping the reference junction in an ice bath. This method is usually not convenient for laboratory or industrial environments. Another way to compensate for the voltage introduced at the reference junction is to use an electronic ice point reference. The electronic ice point reference is a resistive circuit which creates a voltage equal to a $0°$ reference temperature voltage. The temperature can then be read directly from standard tables.

Software compensation requires continuously measuring the temperature of the reference junction. The corresponding voltage of the reference junction temperature is used in the law of intermediate temperatures [7]:

$$V_{s,0} = V_{s,r} + V_{r,0}, \tag{A.2}$$

where $V_{s,0}$ is the equivalent voltage of the absolute temperature of the sensing junction, $V_{s,r}$ is the equivalent voltage of the temperature difference between the sensing junction and the reference junction (the output of the thermocouple circuit), and $V_{r,0}$ is the equivalent voltage of the absolute temperature of the reference junction. $V_{s,0}$ is the voltage of interest and will give the desired temperature. For example, if the

reference junction is at $80°C$, the first step would be look up its corresponding output on a thermocouple table ($V_{r,0}$). This value would be added to the output measured by the voltmeter ($V_{s,r}$). The sum of the two values ($V_{s,0}$) has a corresponding absolute temperature found on the thermocouple table.

The benefits of hardware compensation are that the response is faster because there is no computation time. However each different type of thermocouple requires different hardware because they have different output-temperature curves. Software compensation is the opposite. It requires computer manipulation time, but has the versatility of accepting any thermocouple type.

There exist several standard thermocouple types. Table A.1 summarizes the characteristics of the most commonly used thermocouples [11]. Other types exist for use in higher temperature ranges. ($> 1000°C$). Chromel is the trade name for the

Table A.1
Common Thermocouple Characteristics

ANSI Sym.	Type	Range [$°C$]	Standard Error Limits	Special Error limits
T	Copper-Constantan	0-350	$\pm 1.0°C$ or $\pm 0.75\%$	$\pm 0.5°C$ or $\pm 0.4\%$
J	Iron-Constantan	0-750	$\pm 2.2°C$ or $\pm 0.75\%$	$\pm 1.1°C$ or $\pm 0.4\%$
E	Chromel-Constantan	0-900	$\pm 1.7°C$ or $\pm 0.5\%$	$\pm 1.0°C$ or $\pm 0.4\%$
K	Chromel-Alumel	0-1250	$\pm 2.2°C$ or $\pm 0.75\%$	$\pm 1.1°C$ or $\pm 0.4\%$
Sub-Zero Range				
T	Copper-Constantan	-200-0	$\pm 1.0°C$ or $\pm 1.5\%$	Not Established
E	Chromel-Constantan	-200-0	$\pm 1.7°C$ or $\pm 1.0\%$	Not Established
K	Chromel-Alumel	-200-0	$\pm 2.2°C$ or $\pm 2.0\%$	Not Established

chromium-nickel alloy used in Type K and Type E thermocouples. Constantan is the trade name for the copper-nickel alloy used in Type E, Type J, and Type T thermocouples. Figure A-4 shows the milivolt output of the thermocouples vs. temperature [11].

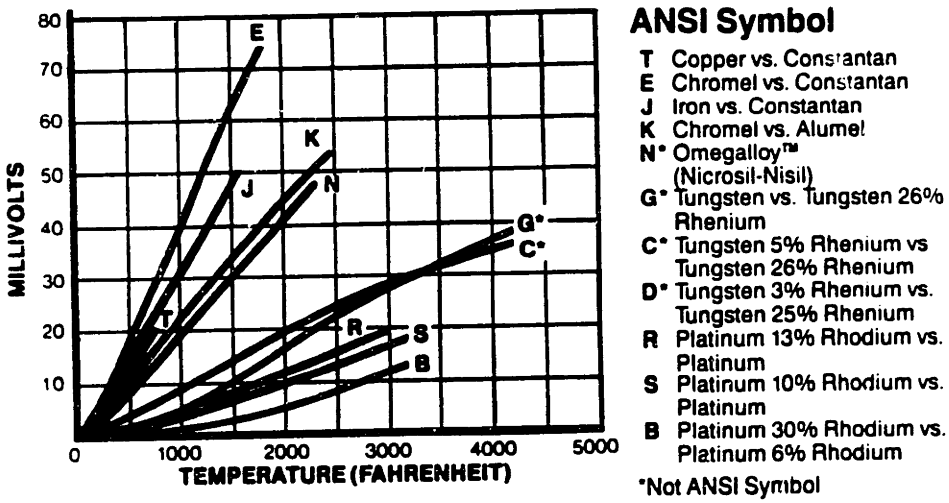

Figure A-4: Thermocouple Output Versus Temperature

Types T, J, E, and K are the most commonly used. Type E thermocouples are most sensitive. Type T thermocouples have the smallest range.

Appendix B

Thermal Experiment Computer Programs

B.1 Sample Motor Control Program

```
;TEMP1.CMD
;MOTOR MOVES BACK AND FORTH IN Y DIRECTION
;UNITS IN INCHES
;START MOTOR IN X = ANY COORDINATE, Y = SMALL
;COORDINATE (ENOUGH TO TRAVEL)
;THIS PROGRAM IS BASED ON RELATIVE POSITIONS

;CONVERSION FROM MICROSTEPS TO INCHES
;(AMP SET AT 125 MICROSTEPS/STEP)
UU012500/1

;SET VELOCITY TO 15 IN/S
VELO 15.0
;SET ACCELERATION 200 IN/S^2
ACCO 0.2
```

```
;B1 SUBROUTINE ARE THE MOTIONS OF THE PATTERN
:B1
;MOVE Y AXIS +15 IN
MRI2 15.0
;WAIT FOR Y AXIS TO FINISH MOTION
WX2
;MOVE Y AXIS -15 IN
MRI2 -15.0
;WAIT FOR Y AXIS TO FINISH MOTION
WX2
;REPEAT
JUMP B1
```

Figure B-1: Motion Control Program: Y Direction 15 Inches, Trapezoidal Velocity Profile

```
;TEMP2.CMD
;MOTOR MOVES BACK AND FORTH IN X AND Y DIRECTIONS
;UNITS IN INCHES
;START MOTOR IN X = LARGE COORDINATE, Y = SMALL
;COORDINATE (ENOUGH TO TRAVEL)
;THIS PROGRAM IS BASED ON RELATIVE POSITIONS

;CONVERSION FROM MICROSTEPS TO INCHES
;(AMP SET AT 125 MICROSTEPS/STEP)
UU012500/1

;SET VELOCITY TO 15 IN/S
VELO 15.0
;SET ACCELERATION 200 IN/S^2
ACCO 0.2

;B1 SUBROUTINE ARE THE MOTIONS OF THE PATTERN
:B1
;MOVE X AXIS -8 IN, Y AXIS +8 IN
MR2 8.0
MR1 -8.0
GO
;WAIT FOR X, Y AXES TO FINISH MOTION
WX2
WX1
;MOVE X AXIS +8 IN, Y AXIS -8 IN
MR2 -8.0
MR1 8.0
GO
;WAIT FOR X, Y AXES TO FINISH MOTION
```

```
WX1
WX2
;REPEAT
JUMP B1
```

Figure B-2: Motion Control Program: XY Direction 8 Inches, Trapezoidal Velocity Profile

B.2 Data Acquisition BASIC Program

```
10 '*****************************************************************
30 '*          TEMP.BAS - Temperature Data Acquisition Program      *
40 '*  Irene Chow                                  3/1/92           *
50 '*****************************************************************
55 'ADAPTED FROM METRABYTE CORPORATION
57 'PROGRAM EX3.BAS FOR DAS-20 BOARD
80 '----------- INITIAL SCREEN PRE-AMBLE -------------------------
90 SCREEN 0,0,0:WIDTH 80:CLS: KEY OFF
110 '----- STEP 1: Load DAS20.BIN driver by contracting workspace
120 CLEAR, 49152!
130 DEF SEG = 0
140 SG = 256 * PEEK(&H511) + PEEK(&H510)
150 SG = SG + 49152!/16
160 DEF SEG = SG
170 BLOAD "DAS20.BIN", 0
190 '----- STEP 2: Initialize with mode 0 ------------------------
200 DIM DIO%(10)
210 OPEN "DAS20.ADR" FOR INPUT AS #1  'get base I/O address
220 INPUT #1, DIO%(0)
230 DIO%(1) = 2                       'interrupt level
240 DIO%(2) = 1                       'D.M.A. level
260 FLAG% = 0                         'error variable
270 MD% = 0                           'mode 0 - initialize
280 CALL DAS20 (MD%, DIO%(0), FLAG%)
290 IF FLAG%<>0 THEN PRINT "INSTALLATION ERROR":STOP 'Halt on error
310 '----- STEP 3: Prompt for scan sequence and set using mode 1 --
330 INPUT "Enter channel number         : ",L%
340 INPUT "Enter gain range             : ",U%
```

```
350 INPUT "Enter 2-first, 0-next, 1-last: ",C%
360 DIO%(0)=L%                          'set channel
370 DIO%(1)=U%                          'set gain range
380 DIO%(2)=C%                          'set command
390 MD% = 1                             'mode 1 - set scan sequence
400 CALL DAS20 (MD%, DIO%(0), FLAG%)
410 IF FLAG%<>0 THEN PRINT "Error #";FLAG%;" in setting scan
sequence":STOP
420 IF C% <> 1 THEN GOTO 330
430 '
440 '----- STEP 4: Report on scan sequence, view queue mode 2 -----
450 DIM DSEQ%(100)
460 N = 0
470 DIO%(2) = 2
480 MD% = 2                               'mode 2 - view queue
490 CALL DAS20 (MD%, DIO%(0), FLAG%)
500 IF FLAG%<>0 THEN PRINT "Error #";FLAG%;" in mode 2":STOP
510 PRINT USING "channel = ## gain = ## command = #";
DIO%(0),DIO%(1),DIO%(2)
520 DSEQ%(N) = DIO%(0)
530 DSEQ%(N+1) = DIO%(1)
540 N = N+2
550 IF N >= 100 THEN GOTO 590
560 IF DIO%(2) <> 1 THEN GOTO 480
580 '----- STEP 5: Do one A/D conversion using mode 3 -----------
590 FILEN$ = "TEST12.DAT"
600 OPEN "O", 2, FILEN$
610 TIME$ = "0:0"
620 FOR I = 0 TO 1920
630 MD% = 3                         'mode 3 - do one A/D conversion
```

```
640 DIO%(0) = 0
650 DIO%(1) = 0
660 CALL DAS20 (MD%, DIO%(0), FLAG%)
670 IF FLAG%<>0 THEN PRINT "Error #";FLAG%;" in mode 3":STOP
675 GOSUB 1000
680 PRINT USING "Channel ## reads #####.## deg";DIO%(1),F
685 PRINT TIMER
690 PRINT #2, C;TIMER
692 IF I < 120 GOTO 695
693 GOTO 698
695 FOR A = 0 TO 5700
696 NEXT A
697 GOTO 700
698 FOR A = 0 TO 85500!
699 NEXT A
700 NEXT I
705 CLOSE #2
710 END
990 'Convert Degrees C then to Degrees F to print to screen
1000 C = DIO%(0) / 10.24
1030 F = C*9!/5! + 32!
1050 RETURN
```

Figure B-3: BASIC Temperature Data Acquisition Program

Appendix C

Motion Control Equation Derivations

C.1 Constant Acceleration Velocity Profiles

C.1.1 Condition for Triangular Velocity Profile

If the distance specified does not allow the motor to accelerate to the specified peak velocity in half the the specified distance, the motor does not reach the peak velocity. The result is a triangular velocity profile. The distance traveled by the motor during acceleration and deceleration is given by:

$$s_1 = s_3 = \frac{1}{2} a_s T_1^2. \tag{C.1}$$

In order for the motor to reach peak velocity, the specified distance must be greater than the distance traveled during acceleration and deceleration:

$$\begin{aligned} s_{tot} &> s_1 + s_3 && \text{(C.2)} \\ &> \frac{1}{2} a_s T_1^2 + \frac{1}{2} a_s T_1^2 && \text{(C.3)} \\ &> a_s T_1^2. && \text{(C.4)} \end{aligned}$$

Substituting

$$T_1 = \frac{V_p}{a_s} \tag{C.5}$$

into equation C.4 gives the condition for trapezoidal velocity curve:

$$s_{tot} > \frac{V_p^2}{a_s}. \tag{C.6}$$

C.2 Linear Acceleration Velocity Profiles

C.2.1 General Case

This analysis begins by considering only the parabolic portion of the velocity profile. The velocity of the motor is parabolic except after it reaches the peak velocity. Since the velocity is quadratic, the position (integral of velocity) of the motor will have the form

$$s = \alpha t^3 + \beta t^2 + \gamma t + \delta, \tag{C.7}$$

where α, β, γ, and δ are constant coefficients. It follows that the velocity will be of the form:

$$v = \frac{ds}{dt} = 3\alpha t^2 + 2\beta t + \gamma, \tag{C.8}$$

and that the acceleration will have the form:

$$a = \frac{dv}{dt} = 6\alpha t + 2\beta. \tag{C.9}$$

The boundary conditions are:

$$s(0) = 0 \tag{C.10}$$

$$v(0) = 0 \tag{C.11}$$

$$a(0) = a_s. \tag{C.12}$$

These boundary conditions determine the constants δ, γ, and β, respectively:

$$\delta = 0 \tag{C.13}$$

$$\gamma = 0 \tag{C.14}$$

$$\beta = \frac{a_s}{2}. \tag{C.15}$$

Substituting equations C.13 through C.15 into equations C.7 through C.9 gives the general equations:

$$s = \alpha t^3 + \frac{a_s}{2} t^2 \tag{C.16}$$

$$v = 3\alpha t^2 + a_s t \tag{C.17}$$

$$a = 6\alpha t + a_s \tag{C.18}$$

From this point the analysis branches depending on whether or not the distance specified gives the motor enough room to accelerate to the specified peak velocity.

C.2.2 Smooth Velocity Profile

In the case where the motor has exactly the distance needed to accelerate to the specified velocity, its velocity will follow one parabola. It will reach the peak velocity at the top of the parabola. The time period T_2 will equal zero. In the case where the motor has more than the distance needed, its velocity will follow the parabola up to the specified peak speed (during T_1). Then it will cruise at the peak speed (during T_2), and finally follow the same parabola shifted by T_2 to the right (during T_3). The added boundary condition in both of these cases is:

$$a(T_1) = 0. \tag{C.19}$$

This boundary condition determines α:

$$\alpha = -\frac{a_s}{6T_1}. \tag{C.20}$$

To find T_1, a fifth boundary condition is required:

$$v(T_1) = V_p. \tag{C.21}$$

Substituting equations C.20 and C.21 into equation C.17 yields T_1:

$$T_1 = \frac{2V_p}{a_s}. \tag{C.22}$$

Substituting equation C.22 into equation C.20 gives α:

$$\alpha = -\frac{a_s^2}{12V_p}. \tag{C.23}$$

Therefore the equations for the smooth velocity profile during acceleration are:

$$s = -\frac{a_s^2}{12V_p}t^3 + \frac{1}{2}a_s t^2 \tag{C.24}$$

$$v = -\frac{a_s^2}{4V_p}t^2 + a_s t \tag{C.25}$$

$$a = -\frac{a_s^2}{2V_p}t + a_s. \tag{C.26}$$

These equations hold for the entire time of motion in the case where the motor reaches the peak velocity at exactly half the distance specified. During T_2 of the smooth velocity profile, the following equations hold:

$$s = s_1 + V_p(t - T_1) = \frac{2V_p^2}{3a_s} + V_p t \tag{C.27}$$

$$v = V_p \tag{C.28}$$

$$a = 0. \tag{C.29}$$

During T_3 the equations are the same as for T_1, but they are shifted by T_2:

$$s = -\left(\frac{a_s^2}{12V_p}\right)\left(t - \frac{s_{tot}}{V_p} + \frac{8V_p}{3a_s}\right)^3 + \frac{1}{2}a_s\left(t - \frac{s_{tot}}{V_p} + \frac{8V_p}{3a_s}\right)^2 \tag{C.30}$$

$$v = -\left(\frac{a_s^2}{4V_p}\right)\left(t - \frac{s_{tot}}{V_p} + \frac{8V_p}{3a_s}\right)^2 + a_s\left(t - \frac{s_{tot}}{V_p} + \frac{8V_p}{3a_s}\right) \quad \text{(C.31)}$$

$$a = -\left(\frac{a_s^2}{2V_p}\right)\left(t - \frac{s_{tot}}{V_p} + \frac{8V_p}{3a_s}\right) + a_s \quad \text{(C.32)}$$

C.2.3 Condition for Parabolic Velocity Profile

If the distance specified does not allow the motor to accelerate to the specified velocity, a parabola is fit to reach the peak velocity reached by following the original parabola. The condition for the the motor to have enough room to accelerate is:

$$s_{tot} > s(T_1 + T_3). \quad \text{(C.33)}$$

Substituting $2T_1$ into equation C.24 gives the condition for a smooth profile to occur:

$$s_{tot} > -\frac{a_s^2}{12V_p}(sT_1)^3 + \frac{a_o}{2}(2T_1)^2. \quad \text{(C.34)}$$

Substituting

$$T_1 = \frac{2V_p}{a_s} \quad \text{(C.35)}$$

into equation C.34 gives the condition for smooth velocity curve:

$$s_{tot} > \frac{16V_p^2}{3a_s}. \quad \text{(C.36)}$$

C.2.4 Parabolic Velocity Profile

The parabolic profile follows the general case. The fourth boundary condition in this case is:

$$v(T_3) = 0. \quad \text{(C.37)}$$

This boundary condition determines α:

$$\alpha = -\frac{a_s}{3T_3} \quad \text{(C.38)}$$

To find T_3 a fifth boundary condition is required:

$$s(T_3) = s_{tot}. \tag{C.39}$$

Substituting equations C.38 and C.39 into equation C.16 yields T_3:

$$T_3 = \sqrt{\frac{6s_{tot}}{a_s}}. \tag{C.40}$$

Substituting equation C.40 into equation C.38 gives α:

$$\alpha = -\frac{\sqrt{6}a_s^{1.5}}{18\sqrt{s_{tot}}}. \tag{C.41}$$

Therefore the equations of motion for the parabolic velocity profile at all times are:

$$s = \left(\frac{\sqrt{6}a_s^{1.5}}{18\sqrt{s_{tot}}}\right) t^3 + a_s t^2 \tag{C.42}$$

$$v = \left(\frac{\sqrt{6}a_s^{1.5}}{6\sqrt{s_{tot}}}\right) t^2 + a_s t \tag{C.43}$$

$$a = \left(\frac{\sqrt{6}a_s^{1.5}}{3\sqrt{s_{tot}}}\right) t + a_s \tag{C.44}$$

Appendix D

Linear Variable Differential Transformers

D.1 Basic Principles of Operation

The Linear Variable Differential Transformer (LVDT) is a mutual inductance transducer. It produces a voltage output proportional to the displacement of its ferromagnetic core. Figure D-1 shows the operation of an LVDT.

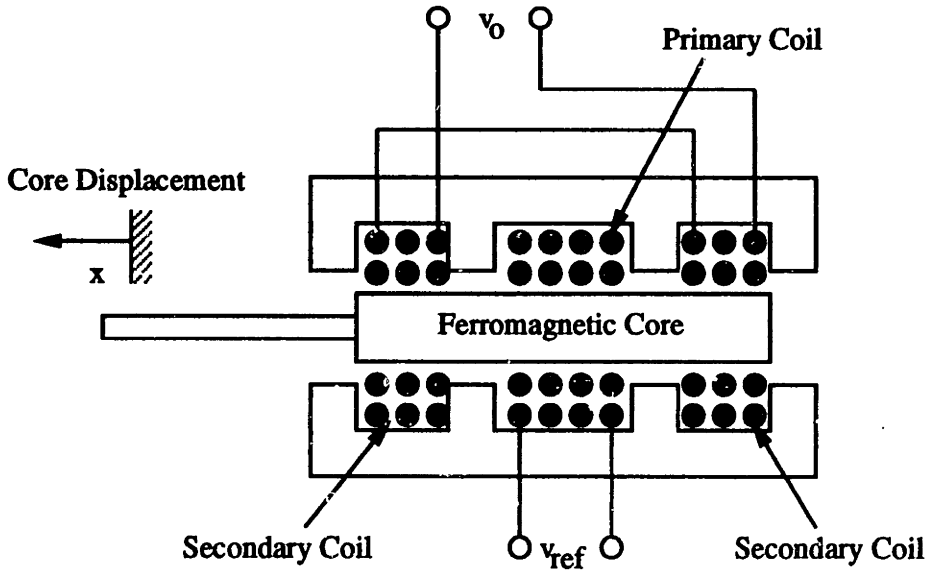

Figure D-1: LVDT Operation

The LVDT consists of a primary coil and two secondary coils. An AC excitation

applied to the primary coil induces an AC voltage in the secondary coils. The polarities of the induced voltages in the secondary coils are opposite. The output of the LVDT is the difference between these two voltages. The core provides a flux linkage path. Changing the position of the core changes the flux path. When the core is centered between the two secondary coils, the output of the LVDT is zero (null position). If the core is displaced, the induced voltage of the coil towards which it moves increases, while the induced voltage of the other coil decreases. Therefore, the LVDT outputs the direction of displacement as well as the amount of displacement. The output amplitude of the LVDT is a voltage that varies linearly with the displacement. However, at the ends of the core travel, the linearity decreases. Figure D-2 shows the voltage output as a function of the displacement.

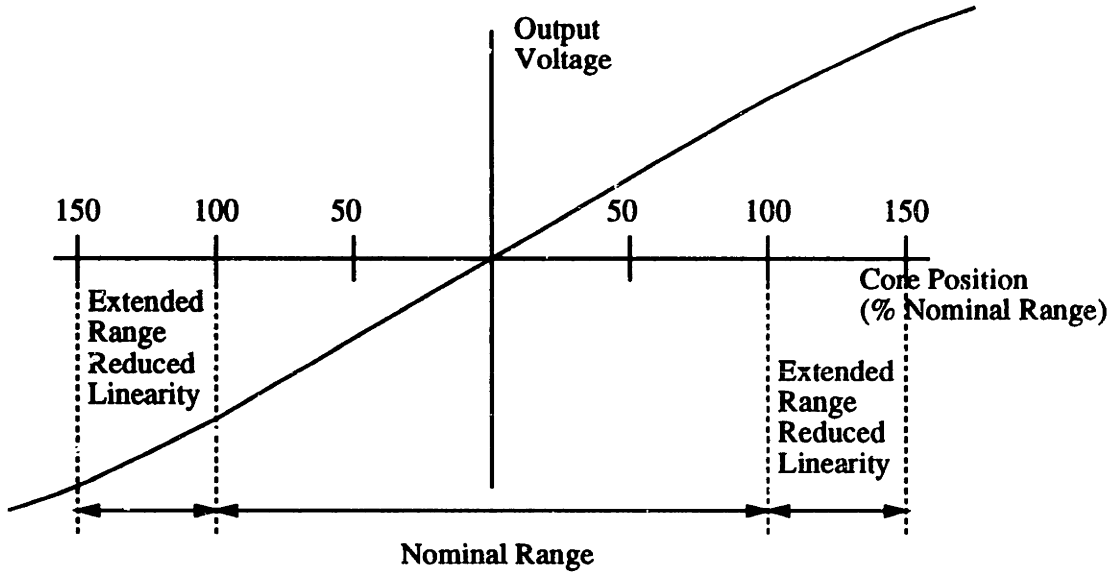

Figure D-2: LVDT Output

D.2 The DC-LVDT

The DC-LVDT allows for DC operation. It consists of an AC-operated LVDT and a carrier generator/signal conditioning module. Figure D-3 shows a block diagram of the module [6]. The module accepts a DC voltage input. A carrier oscillator within the module converts the DC input to the constant amplitude sine wave required by

the AC-LVDT. The module also demodulates and amplifies the LVDT output, to provide a linear DC voltage output proportional to the position of the core. The power supply common is also the the ground for the DC output.

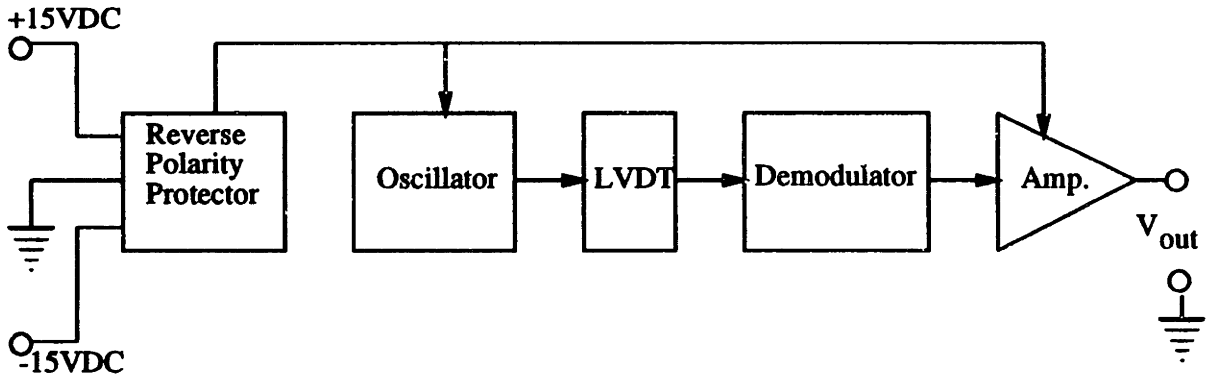

Figure D-3: DC-LVDT Module

Appendix E

Motion Control Experiment Computer Programs

E.1 Sample Motor Control Programs

```
;LVDT1.CMD
;TRAPEZOIDAL VELOCITY PROFILE
;MOTOR MOVES BACK AND FORTH IN Y DIRECTION
;UNITS IN INCHES
;ROTATE MOTOR CLOCKWISE 90 DEGREES
;START MOTOR IN X = COORDINATE SO TRAVEL
;WILL BE IN LINEAR RANGE OF LVDT
;Y = LINED UP WITH LVDT
;THIS PROGRAM IS BASED ON RELATIVE POSITIONS

;CONVERSION FROM MICROSTEPS TO INCHES
;(AMP SET AT 125 MICROSTEPS/STEP)
UU012500/1

;SET X AXIS VELOCITY AND ACCELERATION
;LOW TO PREVENT ACCIDENTAL MOTION IN
```

```
;X DIRECTION
VEL2 0.00008
ACC2 0.00008
;SET Y VELOCITY TO 40 IN/S
VEL1 40.0
;SET Y ACCELERATION TO 250 IN/S^2
ACC1 0.25
;TURN OFF PARABOLIC VELOCITY PROFILE
PARA1-

;B1 SUBROUTINE ARE THE MOTIONS OF THE PATTERN
:B1
;MOVE Y AXIS 15 IN
MRI1 15.0
;WAIT FOR Y AXIS TO FINISH MOTION
WX1
;WAIT 2 SECONDS
WT2000
;MOVE Y AXIS -15 IN
MRI1 -15.0
;WAIT FOR Y AXIS TO FINISH MOTION
WX1
```

Figure E-1: Motion Control Program: Trapezoidal Velocity Profile

```
;LVDT2.CMD
;TRIANGULAR VELOCITY PROFILE
;MOTOR MOVES BACK AND FORTH IN Y DIRECTION
;UNITS IN INCHES
;ROTATE MOTOR CLOCKWISE 90 DEGREES
;START MOTOR IN X = COORDINATE SO TRAVEL
;WILL BE IN LINEAR RANGE OF LVDT
;Y = LINED UP WITH LVDT
;THIS PROGRAM IS BASED ON RELATIVE POSITIONS

;CONVERSION FROM MICROSTEPS TO INCHES
;(AMP SET AT 125 MICROSTEPS/STEP)
UU012500/1

;SET X AXIS VELOCITY AND ACCELERATION
;LOW TO PREVENT ACCIDENTAL MOTION IN
;X DIRECTION
VEL2 0.00008
ACC2 0.00008
;SET Y VELOCITY TO 40 IN/S
VEL1 40.0
;SET Y ACCELERATION TO 100 IN/S^2
ACC1 0.1
;TURN OFF PARABOLIC VELOCITY PROFILE
PARA1-

;B1 SUBROUTINE ARE THE MOTIONS OF THE PATTERN
:B1
;MOVE Y AXIS 15 IN
MRI1 15.0
```

```
;WAIT FOR Y AXIS TO FINISH MOTION
WX1
;WAIT 2 SECONDS
WT2000
;MOVE Y AXIS -15 IN
MRI1 -15.0
;WAIT FOR Y AXIS TO FINISH MOTION
WX1
```

Figure E-2: Motion Control Program: Triangular Velocity Profile

```
;LVDT3.CMD
;SMOOTH VELOCITY PROFILE
;MOTOR MOVES BACK AND FORTH IN Y DIRECTION
;UNITS IN INCHES
;ROTATE MOTOR CLOCKWISE 90 DEGREES
;START MOTOR IN X = COORDINATE SO TRAVEL
;WILL BE IN LINEAR RANGE OF LVDT
;Y = LINED UP WITH LVDT
;THIS PROGRAM IS BASED ON RELATIVE POSITIONS

;CONVERSION FROM MICROSTEPS TO INCHES
;(AMP SET AT 125 MICROSTEPS/STEP)
UU012500/1

;SET X AXIS VELOCITY AND ACCELERATION
;LOW TO PREVENT ACCIDENTAL MOTION IN
;X DIRECTION
VEL2 0.00008
ACC2 0.00008
;SET Y VELOCITY TO 40 IN/S
VEL1 40.0
;SET Y ACCELERATION TO 600 IN/S^2
ACC1 0.6
;TURN ON PARABOLIC VELOCITY PROFILE
PARA1+

;B1 SUBROUTINE ARE THE MOTIONS OF THE PATTERN
:B1
;MOVE Y AXIS 15 IN
MRI1 15.0
```

```
;WAIT FOR Y AXIS TO FINISH MOTION
WX1
;WAIT 2 SECONDS
WT2000
;MOVE Y AXIS -15 IN
MRI1 -15.0
;WAIT FOR Y AXIS TO FINISH MOTION
WX1
```

Figure E-3: Motion Control Program: Smooth Velocity Profile

```
;LVDT4.CMD
;PARABOLIC VELOCITY PROFILE
;MOTOR MOVES BACK AND FORTH IN Y DIRECTION
;UNITS IN INCHES
;ROTATE MOTOR CLOCKWISE 90 DEGREES
;START MOTOR IN X = COORDINATE SO TRAVEL
;WILL BE IN LINEAR RANGE OF LVDT
;Y = LINED UP WITH LVDT
;THIS PROGRAM IS BASED ON RELATIVE POSITIONS

;CONVERSION FROM MICROSTEPS TO INCHES
;(AMP SET AT 125 MICROSTEPS/STEP)
UU012500/1

;SET X AXIS VELOCITY AND ACCELERATION
;LOW TO PREVENT ACCIDENTAL MOTION IN
;X DIRECTION
VEL2 0.00008
ACC2 0.00008
;SET Y VELOCITY TO 40 IN/S
VEL1 40.0
;SET Y ACCELERATION TO 250 IN/S^2
ACC1 0.25
;TURN ON PARABOLIC VELOCITY PROFILE
PARA1+

;B1 SUBROUTINE ARE THE MOTIONS OF THE PATTERN
:B1
;MOVE Y AXIS 15 IN
MRI1 15.0
```

```
;WAIT FOR Y AXIS TO FINISH MOTION
WX1
;WAIT 2 SECONDS
WT2000
;MOVE Y AXIS -15 IN
MRI1 -15.0
;WAIT FOR Y AXIS TO FINISH MOTION
WX1
```

Figure E-4: Motion Control Program: Parabolic Velocity Profile

E.2 Data Acquisition BASIC Program

```
10 '*************************************************************
20 '*                                                           *
30 '*      LVDT.BAS - LVDT Position Data Acquisition Program     *
40 '*                                                           *
50 '*  Irene Chow                                      4/1/92 *
60 '*************************************************************
65 'ADAPTED FROM METRABYTE CORPORATION
66 'PROGRAM EX4.BAS FOR DAS-20 BOARD
70 '
80 '
90 '----------- INITIAL SCREEN PRE-AMBLE ----------------------
100 SCREEN 0,0,0:WIDTH 80:CLS: KEY OFF
110 '
120 '----- STEP 1: Load DAS20.BIN driver by contracting workspace
130 CLEAR, 49152!
140 DEF SEG = 0
150 SG = 256 * PEEK(&H511) + PEEK(&H510)
160 SG = SG + 49152!/16
170 DEF SEG = SG
180 BLOAD "DAS20.BIN", 0
190 '
200 '----- STEP 2: Initialize with mode 0 ---------------------
210 DIM DIO%(10)
220 OPEN "DAS20.ADR" FOR INPUT AS #1  'get base I/O address
230 INPUT #1, DIO%(0)
240 DIO%(1) = 2                        'interrupt level
250 DIO%(2) = 1                        'D.M.A. level
260 DAS20 = 0                         'call offset - always zero
```

```
270 FLAG% = 0                              'error variable
280 MD% = 0                                'mode 0 - initialize
290 CALL DAS20 (MD%, DIO%(0), FLAG%)
300 IF FLAG%<>0 THEN PRINT "INSTALLATION ERROR":STOP
305 'Halt on error
310 '
320 '--STEP 3: Prompt for scan sequence and set using mode 1 --
330 '
340 INPUT "Enter channel number          : ",L%
350 INPUT "Enter gain range              : ",U%
360 INPUT "Enter 2-first, 0-next, 1-last: ",C%
370 DIO%(0)=L%                             'set channel
380 DIO%(1)=U%                             'set gain range
390 DIO%(2)=C%                             'set command
400 MD% = 1                                'mode 1 - set scan sequence
410 CALL DAS20 (MD%, DIO%(0), FLAG%)
420 IF FLAG%<>0 THEN PRINT "Error #";FLAG%;" in
setting scan sequence":STOP
430 IF C% <> 1 THEN GOTO 340
440 '
450 '----- STEP 4: Set timer rate to trigger A/D using mode 24----
460 'Alternatively you can externally trigger the A/D, in which
470 'case this step can be skipped (see Step 5).
480 '
490 'Setting timer to 200Hz
500 DIO%(0) = 6250 'you can set another rate here if you want,
510 DIO%(1) = 0    'this divides 5MHz by 25,000 (DIO%(0)
520                'if timer word 2 (DIO%(1))=0 then word not used
530 MD% = 24       'mode 24 - timer set
540 CALL DAS20 (MD%, DIO%(0), FLAG%)
```

```
550 IF FLAG%<>0 THEN PRINT "Error #";FLAG%;"
in setting timer":STOP
560 '
570 '----- STEP 5: Do N conversions to array X%(*) --------------
575 'Enter Number of Conversions
580 N = 960 'number of conversions required
590 DIM X%(N-1)              'set up 500 element integer array
600 DIO%(0) = N              'number of conversions required
610 DIO%(1) = VARPTR(X%(0))  'provide array location
620 DIO%(2) = 2 'trigger source/ 0 = external trigger
counter 1 source
625 DIO%(3)=1
630             '   1=internal timer with ext gate
640             '   2=internal timer start as result
650             '     of executing mode 4
660 MD% = 4     'mode 4 - A/D to array program control..
670             'will not return from call until all conversions
680             ' have been made.
690 'Note: If internal timer is selected with external gating,
695 'holding counter 1
700 '      gate low will delay starting conversions.
710 PRINT"Performing ";N;" conversions. Please wait."
720 CALL DAS20 (MD%, DIO%(0), FLAG%)
730 IF FLAG%<>0 THEN PRINT "Error #";FLAG%;" in mode 4":STOP
740 '
750 '--Stop internal timer if running (not always necessary)--
760 ' Needed if Internal timer was select (dio%(2) was a 1 or 2
765 'for Mode 4
770 MD% = 26
780 DIO%(0)=0                  'Stop A/D Timer
```

```
790 CALL DAS20 (MD%, DIO%(0), FLAG%)
800 '
810 '----- STEP 6: Display results-----------------------------
820 'Alternatively here you could file them, turn data into
825 'real urits etc.
823 FILEN$="LVDT20.DAT"
824 OPEN "O", 2, FILEN$
825 DIM VOLTS (N)
830 PRINT"data points are as follows:-"
840 FOR I = 0 TO (N-1)
842 VOLTS(I) = X%(I)*20/4096
850 PRINT VOLTS(I);" ";
855 PRINT #2, VOLTS(I)
860 NEXT I
865 CLOSE #2
870 PRINT:PRINT:END
```

Figure E-5: BASIC LVDT Position Data Acquisition Program

Appendix F

Additional Motion Control Plots

This Appendix contains data from additional experiments not mentioned in the text. Figures F-1 and F-2 show the position and velocity curves for parabolic velocity inputs. Figures F-3 through F-6 show the position versus time curves for the loaded and unloaded experiments mentioned in the text.

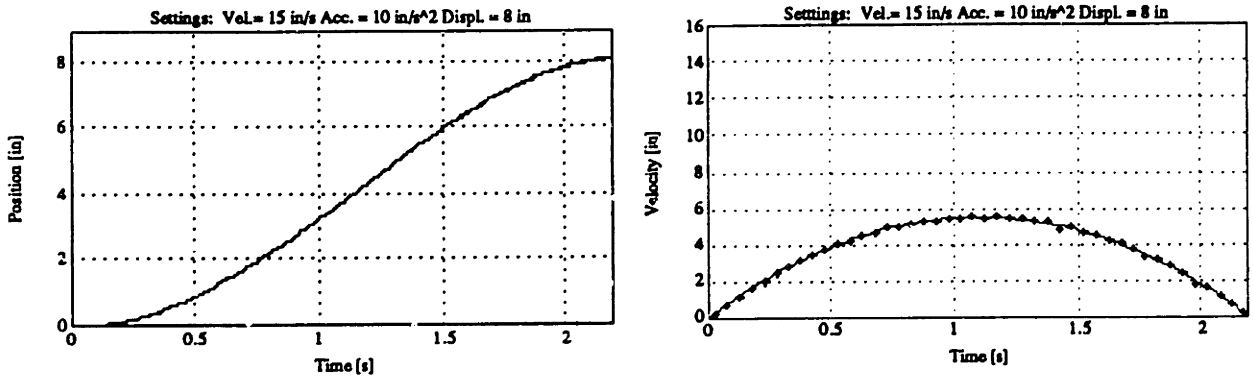

Figure F-1: Parabolic Velocity Profile: Position and Velocity Plots

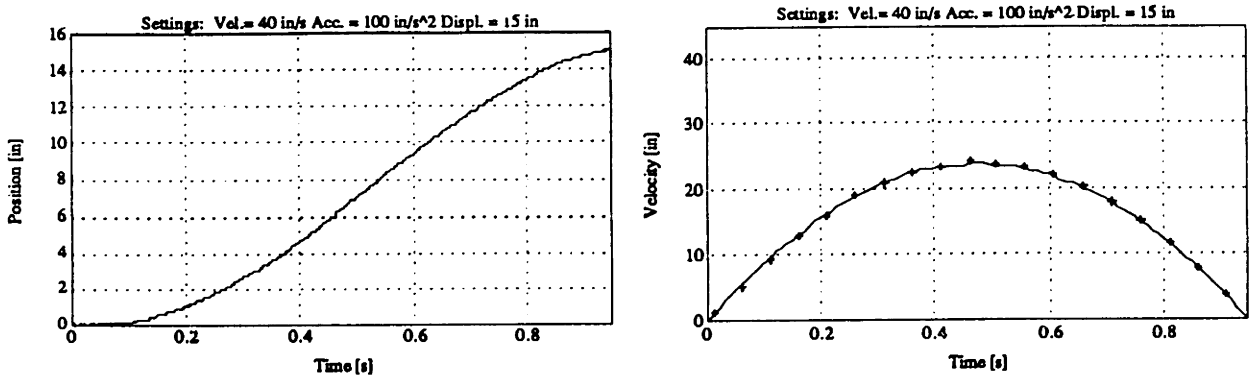

Figure F-2: Parabolic Velocity Profile: Position and Velocity Plots

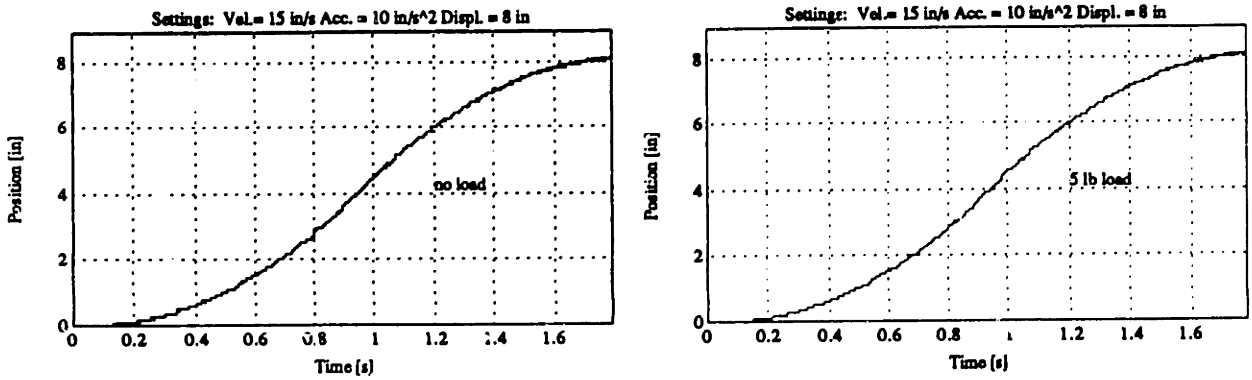

Figure F-3: Trapezoidal Velocity Profile: Position Plots for Loaded and Unloaded

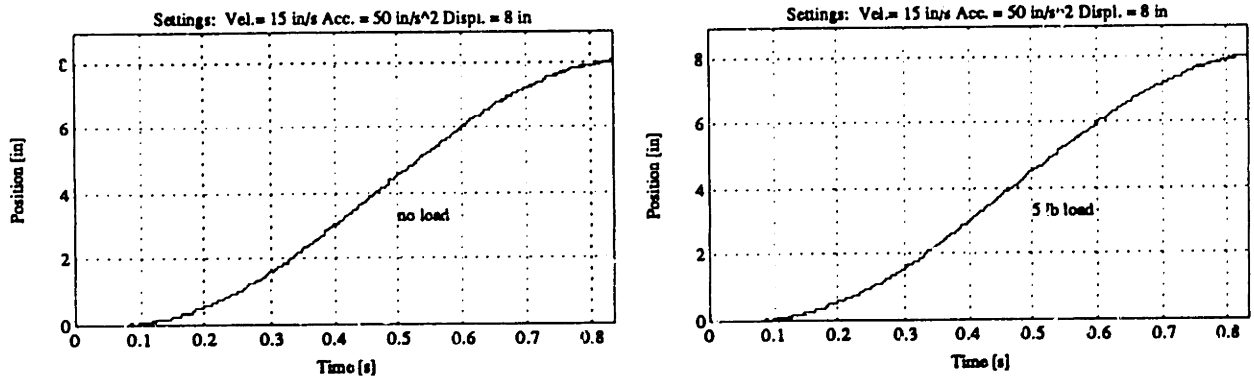

Figure F-4: Triangular Velocity Profile: Position Plots for Loaded and Unloaded

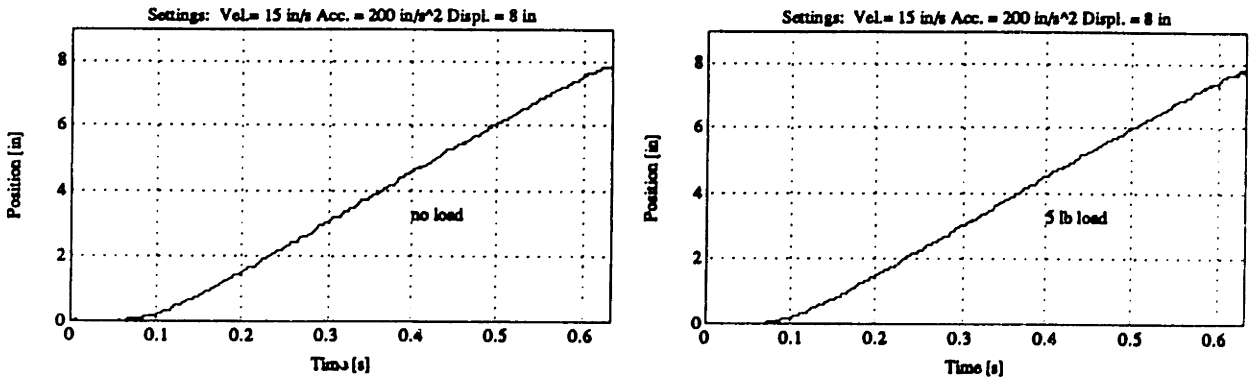

Figure F-5: Smooth Velocity Profile: Position Plots for Loaded and Unloaded

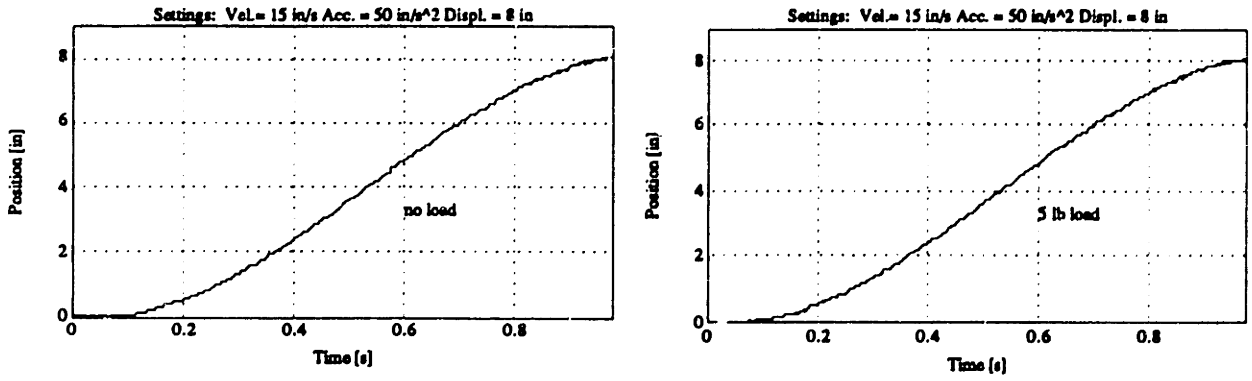

Figure F-6: Smooth Velocity Profile: Position Plots for Loaded and Unloaded

Bibliography

[1] Becker, Martin. *Heat Transfer: A Modern Approach.* New York. (Plenum, 1986).

[2] Crandall, Stephen H., Norman C. Dahl, Thomas J. Lardner. *An Introduction to the Mechanics of Solids.* New York. (McGraw Hill 1979).

[3] De Silva, Clarence W. *Control Sensors and Actuators.* Englewood Cliffs, NJ. (Prentice Hall 1989).

[4] Erturk, Erol. *Evaluation of a New Robotic Assembly Workcell Using Statistical Experimental Techniques and Scheduling Procedures.* Cambridge, MA. (M.I.T., 1991).

[5] Incropera, Frank P. and David P. DeWitt. *Introduction to Heat Transfer.* New York. (John Wiley and Sons 1990).

[6] Lucas Schaevitz. *Linear and Angular Displacement Transducers.* Pennsauken, NJ. (Lucas Schaevitz 1990).

[7] Morris, Alan S. *Principles of Measurement and Instrumentation.* Hemel Hempstead, Hertfordshire, UK (Prentice Hall 1988).

[8] Motion Science, Inc. *Micro Step Motor Drive for Rotary and Linear Step Motors User Guide.* San Jose, CA (Motion Science, Inc. 1989)

[9] Motion Science, Inc. *Motion Processor system and Machine Controller: MoPro IIPC User Guide.* San Jose, CA. (Motion Science, Inc. 1991)

[10] Norton, Harry N. *Sensor and Analyzer Handbook.* Englewood Cliff, NJ. (Prentice Hall, Inc. 1982).

[11] Omega Engineering, Inc. *The Temperature Handbook.* Stamford, CT. (Omega Engineering, Inc. 1991)

[12] Pelta, Edmond R. "Sawyer Motor Positioning Systems, Theory and Practice." *Proceedings of Conference on Applied Motion Control.* Minneapolis, MN. (1986).

[13] Pelta, Edmond R. "Two-Axis Sawyer Motor." *Proceedings of International Conference on Industrial Electronics, Control and Instrumentation.* Milwaukee, WI. (1986).

[14] Rowell, Derek and David N. Wormley. *System Dynamics: An Introduction.* Cambridge, MA. (M.I.T. 1989).

[15] Youcef-Toumi, Kamal. "Sensors." *Robot Manipulators: Analysis, Design and Control Fundamentals.* Cambridge, MA. (McGraw-Hill 1991).

[16] Youcef-Toumi, Kamal and Paul Gjeltema. *A Preliminary Study of A Sawyer Linear Motor.* Cambridge, MA. (M.I.T. Laboratory for Manufacturing and Productivity and Department of Mechanical Engineering, 1991).

[17] Youcef-Toumi, Kamal, Paul Gjeltema, and Irene Chow. *High Speed Robot Manipulation Research Project: Report No. 2.* Cambridge, MA. (M.I.T. Laboratory for Manufacturing and Productivity and Department of Mechanical Engineering, 1992).